A reinterpretation of the Downie Slide (British Columbia, Canada) based on slope damage characterization and subsurface data interpretation

A reinterpretation of the Downie Slide (British Columbia, Canada) based on slope damage characterization and subsurface data interpretation

Davide Donati[1]* (ORCiD: 0000-0003-4083-5910); Allison M. Westin[2] (ORCiD: 0000-0001-6378-8550); Doug Stead[1]; John J. Clague[1]; Thomas W. Stewart[3]; Martin S. Lawrence[4]; Julia Marsh[3]

1 Simon Fraser University, Department of Earth Sciences, Burnaby, British Columbia, Canada

2 Provincial Agricultural Land Commission, Burnaby, British Columbia, Canada

3 BC Hydro and Power Authority, Vernon, British Columbia, Canada

4 BC Hydro and Power Authority, Burnaby, British Columbia, Canada

* Corresponding author: Davide Donati, email: davide_donati@sfu.ca

Funding: This work was supported by the Natural Sciences and Engineering Research Council of Canada [grant number RGPIN 05817] and Forestry Renewal British Columbia Endowment funds provided to Doug Stead.

Conflict of Interest: The authors declare that they have no conflict of interest.

Abstract

The displacement of a large slow-moving landslide is accompanied by slope damage, such as fractures, tension cracks, and slope bulging. Studies of these features provide insight into the mechanisms responsible for the deformation. In this paper, we investigate slope damage at the Downie Slide, a very large landslide in British Columbia, Canada, that is slowly moving along two shear zones sub-parallel to the ground surface. Structural geology, and particularly the morphology of the lower shear zone, strongly controls the deformation and, in turn, the observed internal and surficial slope damage features. We use aerial and underground adit laser scanning and photogrammetry to characterize the geometry of the landslide. We subdivide the slide area into slope damage domains based on the distribution, size, and orientation of the slope damage features. We reconstruct the shape of the two failure surfaces by interpolating borehole inclinometer monitoring data and processing the 3D surfaces in a GIS environment to create aspect and slope maps. We observe a strong correlation between surficial slope damage features and changes in the dip and dip direction of the lower sliding surface. We further infer the presence of a multi-planar failure surface geometry and previously unrecognized structurally controlled damage zones.

1 Introduction

Large complex slow-moving landslides pose a hazard to civil infrastructure and residential areas, particularly in mountainous regions (Petley 2012) where steep slopes are increasingly being developed to accommodate growing populations. Increased demand for resources and energy requires excavation of deeper open pit mines and impoundment of large artificial reservoirs, increasing the potential for major rock slope failures.

Factors conditioning, and mechanisms governing, the behavior of large unstable slopes have been extensively investigated by many authors. The presence and orientation of geological structures, such as faults and folds, may control the location of slope instabilities, as well as potential failure mechanism (e.g., Stead and Wolter 2015). Rock mass quality and discontinuity networks may also affect rock-slope failure mechanisms. At a small scale, slopes formed in a high-quality rock mass with a limited number of widely spaced discontinuity sets may develop local, well defined structurally controlled instabilities. At a large scale, slopes formed in intensely fractured or highly altered rock masses may develop pseudo-circular or multi-planar failure geometries. Highly competent rock masses may also develop rock collapses if irregular rupture surfaces form due to the propagation and coalescence of non-persistent, randomly oriented joints (Hungr et al. 2014; Gschwind et al. 2019). Bedding and foliation commonly act as basal release surfaces for rock slope failures due to their high persistence (Stead and Wolter 2015). Ductile tectonic structures (i.e., folds) and associated jointing can also provide kinematic release for major rockslides (Badger 2002). The 1963 Vajont Slide in Italy (Massironi et al. 2013) and the 1903 Frank Slide in Alberta, Canada (Humair et al. 2013), are examples of major rockslides that released along the limbs of folds – a syncline and an anticline, respectively. Structural and lithological features that characterize the rock mass of an untsable slope constitute what has been referred to as tectonic or “inherited” damage.

Exogenic and endogenic processes may progressively weaken the properties of a rock mass, decreasing stability and pre-conditioning the slope for failure. Earthquakes and seismic fatigue may result in the initiation and propagation of cracks within the slope (Gischig et al. 2015; Wolter et al. 2016a). Hydro-mechanical fatigue due to seasonal groundwater table fluctuations can cause slow displacements in large landslides (Preisig et al. 2016). Long-term valley exhumation through fluvial or glacial erosion induces the formation and growth of exfoliation joints that can facilitate the detachment of rockslides in alpine environments (Evans and Clague 1999; Leith 2012). Glacier retreat may provide kinematic freedom for the activation of deep-seated rock slope deformation (Kos et al. 2016; Clayton et al. 2017) that may lead to catastrophic failure (Roberti et al. 2018). These geological and physical phenomena drive long-term slope degradation referred to as “progressive failure” (Eberhardt et al. 2001). Progressive deterioration of the stability of a slope is associated with the formation of internal and surface features referred to as “slope damage” (Stead and Eberhardt 2013). Counterscarps, double ridges, and grabens are slope damage features typically associated with the evolution of deep-seated gravitational slope deformations (DSGSDs) in alpine environments (Agliardi et al. 2001, 2013a). During deformation of rock slopes, tension cracks may form and propagate at the rear boundary of unstable areas, providing kinematic release and the potential for catastrophic slope

failure (Semenza and Ghirotti 2000; Roberti et al. 2018). Tension cracks can also form in the aftermath of large failures due to stress relaxation (Humair et al. 2013) and locally within slow-moving landslides (Massey et al. 2013). Kink bands and rock mass comminution (Lo and Feng 2014) further induce localized decreases in rock mass quality (Agliardi et al. 2013b). Brittle fracturing of intact rock may form uninterrupted planar or stepped rupture surfaces that provide kinematic freedom for unstable blocks to move (Elmo et al. 2018), with the potential for a significant change in the failure mechanism of the landslide (Adhikary et al. 1997; Donati et al. 2019; Glueer et al. 2019). At smaller scales, the deformation of brittle rock may result in the formation of "gravity-induced" discontinuity sets (Paronuzzi and Bolla 2015; Bolla and Paronuzzi 2020) that decrease rock mass quality. When time-dependent slope deformation (i.e., creep) occurs, cracks can propagate in sub-critical conditions, considerably decreasing the stress magnitude at which damage can form and accumulate (Kemeny 2003). Human activity, for instance through the impoundment of reservoirs, excavations, and mining activity, can also promote slope deformation (Benko and Stead 1998; Semenza and Ghirotti 2000). Finally, lithological and structural features can cause slope damage to accumulate where acting as lateral kinematic constraints (Stead and Eberhardt 2013) or forming complex (non-planar and non-circular) basal sliding surfaces (Kvapil and Clews 1979).

A comprehensive characterization of an unstable slope involves geomorphic, structural, lithological, and hydrogeological investigations. In recent decades, technological advances in remote sensing techniques have enhanced the ability of engineers and geoscientists to collect large datasets, even in inaccessible areas. Airborne and terrestrial laser scanning (ALS/TLS) and photogrammetric techniques, such as terrestrial digital photogrammetry (TDP) and Structure-from-Motion (SfM), can be employed to produce three-dimensional models that incorporate discontinuity and damage data at a variety of scales (Sturzenegger and Stead 2009; Westoby et al. 2012) and facilitate identification and mapping of lineaments and structures (Jaboyedoff et al. 2012; Francioni et al. 2018). Characterizing the type, spatial distribution, and orientation of slope damage features can also provide important insight into the geological processes that control the instability (Donati 2019). Stead and Eberhardt (2013) proposed a distinction between "external" (i.e., surficial) and "internal" slope damage, depending on whether or not the features are visible at the ground surface. Slope damage can also be expressed as "focused" (i.e., localized) or "distributed" to describe the relative distribution of slope damage features throughout the slide mass. Finally, the character of the slope damage can be expressed as "tensile" or "shear" based on the types of mechanisms that generate slope damage.

In this paper, we characterize slope damage at Downie Slide, a very large, slow-moving landslide in southeastern British Columbia, Canada. We investigate the factors and processes that have affected the evolution and spatial distribution of slope damage by taking advantage of a large and comprehensive dataset, which includes remote sensing, geomorphic, geomechanical, subsurface, and monitoring data, to highlight the role of the inherited structures on the long-term evolution of the slope. Based on the results of the slope characterization, we provide a reinterpretation of the mechanisms controlling the evolution and stability of the landslide.

2 The Downie Slide

2.1. Geological, structural, and hydrogeological overview

The Downie Slide is a very large, composite, extremely slow-moving rock slide (Kalenchuk et al. 2013) located on the east slope of Pettipiece Ridge along the west shore of Revelstoke Reservoir in the Columbia River valley (Fig. 1a, b). The slide has a surface area of about 9 km^2; it is 2.4 km long in the north-south direction and 3.2 km long in the east-west direction. The maximum thickness of the displaced rock mass is about 250 m, and its estimated volume is 1.4 billion m^3 (Moore 1989). The unstable slope extends from an original ground surface elevation of 507 m below Revelstoke Reservoir to 1520 m a.s.l. on Pettipiece Ridge. It slopes towards the east at an average angle of 18°, increasing to over 40° at its toe (Piteau et al. 1978). Two subsurface shear zones subparallel to the slope have been identified: a lower shear zone (LSZ) and an upper shear zone (USZ), located at maximum depths of 250 m and 120 m, respectively (Moore 1989). The slide area is bounded along the west and south sides by subvertical scarps up to 125 m high. In contrast, the north boundary of the slide is demarcated by a significantly less prominent side scarp and a wide zone of distributed lateral shear. The toe of the slide is submerged beneath the waters of theRevelstoke Reservoir. Filling of the reservoir began in the fall of 1983, inundating the Columbia River valley floor at ~507 m a.s.l. (roughly coincident with the daylighting elevation of the LSZ). By the summer 1984, the reservoir had completely filled and its water level was 573 m a.s.l. The time of initiation of the landslide is estimated to be between 10,000 years and 7960 years ago based on radiocarbon dating (Piteau et al. 1978; Stantec 2009). Since then, the slide mass has moved up to 300 m downslope toward the Columbia River (Moore 1989).

The Downie Slide is seated within schist, gneiss, quartzite, and marble of the Monashee Complex, a succession of moderate to high-grade Proterozoic to Lower Paleozoic metamorphic rocks locally intruded by granitic plutons (Read and Brown 1981). Geological formations of the Selkirk Allochthon, which crop out on the east side of the Columbia Valley, comprise low- to high-grade metamorphic rocks that were transported tens of kilometers eastward over the Monashee Complex in Middle to Late Jurassic time along the Columbia River Fault Zone (CRFZ), also known as the Monashee Decollement. Lithospheric uplift and arching contributed to subsequent erosion of the region during the Paleogene and to exhumation of the Monashee Complex, which represents a structural window bounded by the Selkirk Allochthon to the east and the Shuswap Metamorphic Complex to the north (Read and Brown 1981). The Columbia River Fault dips towards the east at an angle of between 20° and 30°, and forms a cataclastic damage zone up to 1 km wide (Fig. 1c; Brown and Psutka 1980).

Detailed structural analysis has shown that the area surrounding the Downie Slide has experienced three phases of tectonic deformation. Numerous folds have north-striking axes, and the axis of a major monocline that formed during the final deformation phase constitutes the upper part of the western headscarp (Brown and Psutka 1980). The LSZ and USZ comprise thinly foliated beds of schist and have maximum thicknesses of 62 m and 21 m, respectively. Borehole inclinometer plots, however, indicate that the displacements within the two shear zones are

currently occurring along thin layers of gouge (clayey to silty micaceous sand) less than 1 m thick (BC Hydro 1974, 2010). As an example, Figure 2 shows photographs of core and an inclinometer log from borehole S23A (see Fig. 1 for location), and Table 1 summarizes the interpreted thicknesses of the USZ and LSZ based on the downhole inclinometer records.

The landslide surface is irregular (Fig. 3). The upper slope is hummocky, and the rock mass there is disturbed and fragmented. The central part of the slide is characterized by a uniform, relatively smooth surface with no obvious slope damage features. The lower slope is characterized by extensive cracking and deformation. Large fractures are evident in the southern and northern sectors, whereas slope damage in the central sector of the lower slope appears to be more distributed, and there is evidence in that area of surface erosion by water (Fig. 3). Ephemeral ponds are present on the lower and central portions of the slope. The slide mass constricts the width of Revelstoke Reservoir to 220-280 m from 380-430 m outside of the slide area. The minimum reservoir width coincides with two prominent knobs, referred to as North Knob and South Knob, that bulge into the reservoir near the north and south boundaries of the slide (Fig. 3). Prior to impoundment, the Columbia River flowed in a series of rapids across the toe of the slide area (Piteau et al. 1978). In one of the boreholes drilled at the base of the slope, a buried fluvial channel was found below the slide toe (Piteau et al. 1978), suggesting that deformation of the Downie Slide displaced the thalweg of the Columbia River to the east. The southern and western headscarps appear to be structurally controlled, as observed by Kalenchuk et al. (2013), and coincide with a series of linear features forming a large-scale, step-path geometry that provided kinematic freedom for the slide to move. Kalenchuk et al. (2013) suggested that the Downie Slide has grown by retrogression of the headscarp toward the west and north. Westward retrogression of the headscarp may be responsible for the hummocky deposits forming the upper slope, and retrogression toward the north mobilized a portion of slope referred to as the “lobe” (Fig. 3).

Multiple independent aquifers are located at different depths. Piezometric data are routinely collected by BC Hydro to monitor water pressures at different depths, including those of the LSZ and the USZ. Based on the historical dataset obtained from over 100 piezometers, the slide area has been subdivided into three hydrogeological domains: a lower region with the highest borehole density, a central region, and an upper region (Fig. 3). There is a downward pressure gradient throughout the slide body in the lower region. High hydraulic heads and seasonal artesian conditions exist in lower aquifers in the central region. Artesian conditions also seasonally exist below the basal sliding surface; i.e., LSZ (BC Hydro 2010). The upper region is characterized by relatively low piezometric heads above the LSZ. Tunnels excavated within the lower region (i.e., underground Adit 1 and Adit 2, Fig. 3) have lowered the groundwater table by as much as 150 m from its level prior to construction of Revelstoke Dam (BC Hydro 2010). However, this system does not significantly affect the groundwater regime in the central and upper regions, likely due to the distance of the drainage adits from these regions and the compartmentalized nature of the water storage and hydraulic flow within the slide body.

2.2. Summary of historical investigations and monitoring data

The Downie Slide was first recognized in 1956 during investigations for potential dam sites in the Columbia River valley (Piteau et al. 1978). A preliminary geological study of the slide area was undertaken in 1965 to identify the geometry of the slide, its activity, and its failure mechanisms (Piteau et al. 1978). Exploratory boreholes were drilled and geophysical seismic investigations performed to identify the depth of the rupture surface. Targets and survey monuments were installed in 1975 to analyze surface deformation (BC Hydro 2010). Photogrammetric surveys and traditional field work were also conducted (Piteau et al. 1978). Initial stability analyses performed along five sections through the slide indicated a condition of marginal equilibrium for the slope, with factor of safety values ranging from 0.92 to 1.25. As a result, subsurface drainage and monitoring systems were installed prior to construction of the dam (BC Hydro 1987). Between 1973 and 1975, a 266-m-long exploratory horizontal adit (Adit 1) was excavated within the slide mass in a southwest direction (BC Hydro 2010). In 1977, Adit 1 was extended southwards, and a new adit (Adit 2) was excavated towards the north boundary of the slide (Fig. 3). By 1982, over 2400 m of horizontal tunnels and 13,600 m of drain holes had been drilled, and several piezometers and inclinometers had been installed at the site (Imrie et al. 1992). By the end of construction, the lowering of the water table had provided a substantial increase in the factor of safety (averaging +10%) compared to pre-reservoir conditions (BC Hydro 2010).

Intense monitoring activity using borehole inclinometers, survey monuments, extensometers, and piezometers continued at Downie Slide after completion of the dam. The efficiency of the drainage system has gradually decreased since its completion in 1982 (Imrie et al. 1992), causing a slow increase in piezometric head over time (BC Hydro 2009). Between 2006 and 2008, over 4000 m of additional holes were drilled within Adit 1 to restore and maintain its drainage efficiency (BC Hydro 2010).

Today, the Downie Slide remains one of the most instrumented and monitored slopes in the world. Over 50 boreholes have been drilled and instrumented across the slide (BC Hydro, 2010). Presently, 10 piezometers and five inclinometers remain operational. Surface deformation is monitored using 25 survey monuments, 16 of which are installed within the slide area, six along the perimeter, and three on the east bank of the reservoir. The in-situ monitoring instruments are not distributed homogeneously across the slide area; their spatial density on the lower slope is higher than on the upper slope (Fig. 4).

Present-day displacement rates differ considerably throughout the slide area both spatially and with depth. Borehole inclinometer surveys show that displacement rates at depth have been greater along the LSZ (0.15-3.2 mm/year) than along the USZ (0.2-2.0 mm/year). Much higher displacement rates, up to 16 mm/year, have been measured close to the toe, but are limited to a shallow surficial layer of colluvial material (BC Hydro 2010). In some parts of the slide, displacement rates at depth have remained below the detection limit since the start of monitoring in 1965. Table 2 summarizes displacement rates recorded to date by inclinometers that are presently active (see Fig. 4 for the instrument locations). Surface displacements are monitored through annual GPS monument surveys. Rates

between 1 and 58 mm/year have been recorded, except in the toe area, where the maximum rate is 174 mm/year (BC Hydro 2010).

Several morphological zones (slope domains) have been proposed for the Downie Slide based on geomorphic, structural, and displacement evidence. The earliest proposal was that of Piteau et al. (1978), who recognized five domains and identified the central portion of the lower slope as the most active area (Fig. 5a). More recently, Stantec (2009) divided the slide area into eight domains, based on a geomorphic analysis conducted using the bare earth ALS dataset (Fig. 5b). Kalenchuk et al. (2013) subdivided the Downie Slide into 13 morphological zones based on field data and ALS analysis (Fig. 5c). The most recent landslide subdomain subdivision is that of Westin (2017), which was based on the results from an advanced GIS geomorphic analysis that included roughness and curvature characterization and a lineament analysis performed using hillshade, aspect, and slope maps (Fig. 5d).

3 Geomorphological, structural, and geomechanical characterization of the Downie Slide

3.1. Surficial slope damage

We performed a GIS analysis of surficial slope damage on the Downie Slide in ArcGIS 10.5 (ESRI 2017). We used a 2009 ALS dataset that was available for this study to produce slope, aspect, and hillshade maps, from which we could identify and map slope damage features and their orientations and lengths. This analysis allowed us to identify four slope damage domains within the slide area: an upper distributed slope damage domain, a central undamaged domain, a northern slope damage domain, and a southern slope damage domain (Fig. 6). We plotted lineaments within each slope damage domain in rosette diagrams, and for each domain computed slope damage density values (SD_{20}, defined as the ratio of the number of mapped lineaments to the domain surface area) and slope damage intensity values (SD_{21}, defined as the ratio of the total length of mapped lineaments to the domain surface area) (Table 3). In all domains four major lineament trends are evident: trend I (005°), trend II (047°), trend III (098°), and trend IV (156°). We note that the objective of this analysis was not to subdivide the slide area into discrete zones, but rather to the identify regions with representative and well defined slope damage characteristics.

Upper distributed slope damage domain

The upper portion of the slope has a hummocky morphology that is the result of retrogression of the headscarp and accumulation of displaced blocks, including talus, at its base (Kalenchuk et al. 2013; Westin 2017). Large blocks of highly damaged rock are separated by gaping tension cracks and crevices (Fig. 6). The irregular morphology of this domain suggests a strong component of distributed damage and rock mass degradation. Slope damage features are preferentially oriented parallel to trend II.

Central undamaged domain

The central portion of the Downie Slide is an area lacking prominent slope damage features, with a SD_{21} value significantly lower than that of the other domains (Table 3). It is characterized by a relatively gentle slope and uniform morphology that is only interrupted by shallow creeks and gullies. The domain is bounded to the west by the hummocks of the upper distributed damage domain and to the east by a geomorphic scarp that marks the limit of the northern slope damage domain. Lineament intensity (predominantly parallel to trend II and, to a lesser extent, trend IV) gradually increases toward the north margin of the domain, possibly indicating an increase in rock mass damage or erodibility that has resulted in increased surface disturbance (Fig. 6).

Northern slope damage domain

This domain includes the North Knob. A scarp, which crosses the domain in an approximately east-west direction, divides the domain into two sectors. The northern sector is characterized by north-trending linear damage features that are parallel to trends I and IV and locally exceed 5 m in width. Northeast-trending linear damage features, parallel to trend II, are also present in this area. In contrast, the southern sector, which is the most active area within the slide, is characterized by a rough surface lacking obvious discrete damage features. The lack of damage features may suggest the presence of a more intensely fractured rock mass that favors accumulation of distributed damage (Fig. 6).

Southern slope damage domain

The southern slope damage domain, which includes the South Knob, is characterized by extensional damage features preferentially oriented in an east-west direction, i.e. parallel to trend III. A scarp separates this domain from the central undamaged domain. Tensile surficial damage features appear to be related to the intersection of lower order discontinuity sets, creating step-path geometries. The area close to the reservoir displays counterscarps with a north-south to northeast-southwest orientation that probably have resulted from slumping near the toe of the slide (Fig. 6).

3.2. Rock mass characterization

The Downie Slide rock mass was characterized and discontinuities were mapped both at the surface and within the drainage adits. We conducted underground discontinuity mapping inside drainage Adit 1 using both close-range SfM and TLS methods to provide redundancy and allow comparison of these techniques in an underground setting. SfM was performed at three stations within the northern, southern, and main tunnel of Adit 1. At each location, a 4-m-wide strip survey was undertaken using a Canon EOS 5D Mark II, 20 MegaPixel camera with a f=20 mm focal-length lens. Discontinuity mapping was done using CloudCompare (CloudCompare 2.10 2019). The underground TLS survey was performed using a FARO Laser Scanner Focus^{3D} x330. Scans were done from locations separated by about 3 m along sections of the adit that were not covered in shotcrete. Point cloud post-processing, stitching, and registration were completed in Scene (Faro Technologies 2015). We mapped

discontinuities using Polyworks (InnovMetric 2019). A DJI Phantom 4 Quad-copter equipped with a 20 MegaPixel built-in camera provided photographs of a portion of the western part of the upper headscarp for analysis using UAV-SfM (Unmanned Aerial Vehicle-SfM) approach. We used Polyworks to systematically map discontinuities in four windows located in the headscarp. Figures 7 and 8 summarize the locations and the results of the rock slope characterization surveys.

Discontinuity data obtained through the SfM and TLS surveys of the adits were processed in DIPS (Rocscience 2016). Three main discontinuity sets – D1 (23/059 on average), D2 (79/245 on average), and D3 (74/169 on average) – were identified, with D1 parallel to the foliation and the average slope surface orientation. We observed a good agreement between SfM- and TLS-based discontinuity mapping results, with no significant difference between the datasets (Fig. 7b-d). Several bands of thinly foliated, medium- to coarse-crystalline mica schist, sub-parallel to D1, were observed in the adit during the geomechanical survey (Fig. 7e). The two major shear zones probably developed along similar bands (BC Hydro 2010), which are characterized by lower rock mass quality and strength compared to the surrounding material (Fig. 7e).

There is broad agreement between the discontinuity sets mapped in the adits and in the headscarp (Fig. 8), particularly in the case of discontinuity sets D1 and D2. Differences between the structural mapping results may relate to the different detail of the models (higher in the underground adit models) and the structural complexity of the rock mass due to the three deformation phases (i.e., folding) that have been identified.

Discontinuity sets D2 and D3, identified in the underground rock mass characterization, appear to correlate with lineament trends I and III, respectively. This similarity suggests that the large-scale slope surficial slope damage features are controlled, at least partly, by small-scale discontinuities, including rock mass jointing.

4 Borehole data analysis and shear zone reconstruction

We constructed and interpreted the three-dimensional geometry of the two shear zones by interpolating their locations in the borehole inclinometer plots using the software Surfer 14 (Golden Software 2016). For boreholes without inclinometers, we used the central point of the shear zone. The kriging method, used by Kalenchuk et al. (2009) to analyze subsurface data at the Downie Slide, was employed to interpolate the shear surfaces. Due to the spatial differences in the distribution of the instrumented boreholes, the quality of the shear surface reconstruction is higher on the lower slope; uncertainties are larger on the upper slope and toward the boundaries of the slide area. We assumed points at depth below the base of the south and west scarps to better constrain the locations of the shear surfaces near slide boundaries. This approach was used to simulate the continuation of the structures at depth toward the subvertical slopes bounding the slide. It improved the quality of surface interpolation by reducing the root mean square error (RMSE) of the reconstructed surface (RMSE = 0.3 m), compared to an interpolated sliding surface including the base of the cliffs (RMSE=0.5 m). The section aligned in a WSW-ENE direction (Fig. 9b) shows a

decrease in shear zone dip angles in the lower part of the slope, especially in the northern area. The section aligned in a NNW-SSE direction (Fig. 9c) shows that the vertical distance between USZ and LSZ progressively decreases towards the northern boundary. It is presently unclear whether this morphology is controlled by structural or lithological factors, or if it is a result of the higher uncertainty associated with shear zone interpolation near slide boundaries. Figure 10 displays a 3D view of the reconstructed shear zones.

Changes in orientation of the LSZ are in close agreement with the displacement directions recorded by the borehole inclinometers (Fig. 11a). In particular: 1) the northern portion of the LSZ dips to the southeast; 2) the western portion dips to the east, parallel to the ground surface; 3) the southern central portion dips to the northeast; and 4) the LSZ dips to the east along the southern headscarp, but tilts to the southeast below 700 m a.s.l. The LSZ is a multi-planar surface with a lower dip angle (<15°) beneath the lower part of the slope than beneath the central and upper portions of the slope (15° to > 30°) (Fig. 11b). In contrast, the USZ appears to dip uniformly (15-20°) toward the east, with local areas dipping toward the northeast and southeast beneath the lower slope (Fig. 11c, d).

The causes of the spatial differences in dip angle and dip direction of the shear zones are not well understood. In view of the complex tectonic history of the area, it is possible that the shear zone morphology is partly controlled by medium- and large-scale folds that developed during the three deformation phases described by Brown and Psutka (1980). The different thicknesses, up to 30 m, of schist beds (which comprise 25% of the stratigraphic column; BC Hydro 1974) across the slide may also have contributed to the development of this complex morphology.

We imported the LSZ and USZ surfaces into ArcGIS 10.5 (ESRI 2017) and, based on the LSZ and the ground surface, calculated a volume of 1×10^9 m^3 for the Downie Slide using a cut-and-fill analysis. This estimate is about 30% lower than the previous volume reported by Piteau et al. (1978), and largely stems from the lower thickness estimate of the slide body beneath the upper slope.

5 Discussion

5.1. Determining landslide evolution through slope damage analysis

Surface slope damage features have been documented by several authors to infer the evolution and dynamics of large landslides (Chigira 1992; Agliardi et al. 2001; Shea and van Wyk de Vries 2008; Jaboyedoff et al. 2013; Wolter et al. 2016b). Based on field mapping and physical modelling, these authors have concluded that the principal factors controlling slope damage accumulation are kinematics, failure mechanism, deformation style, and displacement magnitude. An analysis of internal slope damage is significantly more complex due to the inherent difficulties in data collection and subsurface mapping. However, occurrences within a landslide body of outcrops with well-preserved, gravity-induced structures enable identification and characterization of internal slope damage

features and structures, thus providing insights into deformation internal to a slope (Paronuzzi and Bolla 2015). The ability to drill and extract high-quality rock cores can also provide insight into the location and style of deformation within an extremely slowly moving slope (Chigira et al. 2013).

In this study, we used remote sensing techniques to characterize surficial slope damage and perform rock mass characterization along the headscarp. We inferred internal damage from borehole cores acquired in the 1970s and 1980s and interpreted by BC Hydro geoscientists. The quality of the rock cores and logs available for this study is not comparable to that employed more recently by other investigators (e.g., Chigira et al. 2013), due to the poorer quality of drilling and logging techniques used at Downie Slide 40–50 years ago. Additionally, the cores themselves were not available for this study, as they were lost during a debris slide that buried the building where the cores were stored. Nevertheless, the locations of the shear zones, their thicknesses, and the lithological characteristics of the rock are reliable. Our interpretation of surficial and internal slope damage at the Downie Slide is based on comparison of geomorphic features observed on the maps derived from ALS mapping, the morphology of the shear zones, and the structural setting that characterizes the study area.

As noted earlier in the paper, borehole inclinometer records show that the displacement at depth occurs mainly along the LSZ. Previous investigations using numerical modelling methods (Kalenchuk et al. 2012; Donati et al. 2020) likewise noted that the slide behavior and the present geomorphic configuration of the slope are largely controlled by the morphology of the LSZ. Therefore, in this paper our re-interpretation of the evolution of and factors controlling the Downie Slide are based largely on the morphology of the LSZ, and the surface and internal slope damage features identified and mapped using the remote sensing datasets. Limited attention is given to the role of the USZ, as its effects on the evolution of the slide are deemed to be insignificant (Donati et al. 2020).

5.2. Slope damage interpretation

GIS analyses showed that the LSZ has a multi-planar morphology with a change in the dip angle between the upper and lower slopes. The geometry of the LSZ implies an active-passive failure mechanism for the slide, in which rock mass damage accumulates within the transition zone between the active and passive slide blocks (Kvapil and Clews 1979), also referred to as the Prandtl prism (Mencl 1966). Damage within this zone develops due to secondary shearing and crushing of the rock mass, resulting in heaving and expansion (Kvapil and Clews 1979). In this transition zone, effects on jointed rock masses include dilation and sliding along pre-existing discontinuities, failure of intact rock bridges, and development of step-path geometries. Slope damage within the Prandtl prism is a kinematic requirement for slide movement to initiate (Kvapil and Clews 1979), thus distributed slope damage within the transition zone at the Downie Slide may have happened in the initial stages of slope deformation. The quality of the rock mass forming the lower slope may be affected by its proximity to the Columbia River Fault damage zone, which extends to the toe of the Downie Slide. However, no conclusive evidence exists that the fault zone played a significant role in the evolution or initiation of the Downie Slide (Brown and Psutka 1980).

The thickness of the LSZ increases from 15-20 m in the upper part of the slope to 60 m in the lower part (Fig. 12), as evidenced by the intense rock mass comminution, shearing, and mineral alteration observed in borehole cores (an example from borehole S23A is shown in Fig. 2). This thickening has likely resulted from a combination of factors, including: 1) accumulation of internal slope damage within the transition zone; 2) the activity, in the past, of one or multiple additional sliding surfaces; and 3) large displacements along a potentially undulating surface, which may have sheared large-scale asperities (Stead and Eberhardt 2013), resulting in the progressive accumulation of internal damage along the LSZ. Local variations in the amplitude and spatial distribution of undulations or asperities may also be responsible for the change in thickness of the LSZ.

The intersection between the east- and northeast-dipping planes forming the LSZ trends 080° and can be traced through the axis of the slide area. This zone intersects at a 400-m-wide notch in the headscarp at the junction of the west and north scarps. This intersection is also aligned, in part, with an east-west trending valley (the upper reach of Fissure Creek) and is perpendicular to the Columbia River valley (Fig. 13). These observations suggest that a structural zone, possibly a regional fault (herein called Fissure Creek structure) extends several kilometers west of the slide and is characterized by a zone of increased rock mass damage that potentially controls the geometry of the rupture surface and the secondary retrogression of the Downie Slide headscarp (Fig. 13). In the upper part of the slide, there is a slight misalignment between the inferred Fissure Creek structure and the intersection of the east- and northeast-dipping planes forming the LSZ. It is unclear whether the misalignment is due to local changes in orientation of the structure or to the poor constraint provided by few boreholes on the reconstructed LSZ in this area.

The zone of rock mass damage associated with the inferred Fissure Creek structure as it crosses the slide area and the potential Prandtl prism transition zone intersect in the lower central portion of the slope, which is the most actively deforming part of the Downie Slide (Fig. 14). We hypothesize that a concentration of rock mass and internal slope damage is responsible for higher erosion and displacement rates observed on this part of the slide.

Upper distributed damage domain

The upper portion of the slide includes blocks up to 50-100 m wide bordered by crevices up to 10 m deep, resulting from gradual retrogression of the western cliff (Kalenchuk et al. 2013; Westin 2017). The magnitude of the retrogression is likely equivalent to the lateral extent of the domain, i.e. about 1200 m in the east-west direction, minus the 300 m estimated displacement of the slide since its activation. The domain has a wedge shape controlled by rock mass jointing (particularly D2 and D3) that is also evidenced by the stepped geometry of the headscarp. It is likely that instability in the upper slope occurred as a structurally controlled secondary failure subsequent to deformation of the lower slope. The progressive accumulation of detached blocks and their slower downslope displacement are responsible for the hummocky morphology throughout the domain. This hummocky morphology also obscures any evidence of older damage features that might be directly associated with the Fissure Creek damage zone. Logs from borehole inclinometer surveys located along the east boundary of the domain show that sliding occurs along both the LSZ and USZ in this area. However, there are no boreholes within the upper distributed slope damage domain, hence the depths of the sliding surfaces are poorly constrained there.

We created two profiles through the upper distributed damage domain (Fig. 15b, c). Profile 1, in particular, shows a decrease in the thickness of the slide body, to as little as 100 m, in the upper part of the slope, which appears to agree with the results from geophysical seismic investigations described by Piteau et al. (1978). Profile 2 highlights the undulating surface of the hummocks. The forest density within this domain tends to progressively decrease towards the upper slope (Fig. 1b), suggesting that the age of the hummocks decreases near the western scarp and thus that the retrogression of the headscarp occurred over a relatively long time period. It is likely that each hummock represents the remnants of a significant retrogressive event, with each intervening trough representing the approximate position of a former headscarp, and that most of these events occurred during the period of maximum activity of the slide.

Central undamaged domain

The central portion of the Downie Slide overlies a nearly uniform, planar portion of the LSZ that dips 20° ENE. As a result, the surface morphology is smooth, with no significant surficial damage features (Fig. 16a). The Fissure Creek structural damage zone, mentioned above, crosses the northern part of this domain, with limited evidence of surficial damage except for a gradual increase in surface roughness, which we documented by performing a Vector Ruggedness Measure (VRM) analysis (Hobson 1972; Sappington et al. 2007). This analysis investigated the ruggedness of the surface, regardless of its steepness and orientation (Fig. 16b). The increase in roughness may indicate a higher degree of rock mass damage relative to the rest of the domain, although no subsurface data are available to confirm this hypothesis. The west boundary of the central undamaged domain may represent the original upper limit of the slide, which then retrogressed with the progressive accumulation of detached blocks and the formation of the upper distributed damage domain.

Northern slope damage domain

The dip direction of the LSZ within the northern slope damage domain ranges from east to southeast. North-trending surficial damage features are overlain by tension cracks and crevices that trend northeast (Fig. 17a). We hypothesize that this damage network is the result of a complex deformation process: 1) eastward displacement of the central portion of the slide body, which created north-trending extensional damage features within the Prandtl prism; and 2) a change in displacement direction of the slide body above the southwest-dipping portion of the LSZ.

Downslope from the transition zone, there is a 20 m increase or bulge in elevation, accompanied by extensive east-west cracking and dilational damage (Fig. 17b). This damage may have resulted from uplift, as observed in similar transition zones of other large slow-moving landslides (Kvapil and Clews 1979). A change toward the south from focused surficial slope damage in more competent rock to a relatively more fractured and erodible rock mass, with more distributed damage, may be related to the presence of the Fissure Creek damage zone that crosses the slide area in an east-west direction and intersects the most actively deforming part of the slide (Fig. 17c). Intense rock mass fracturing, deformation, and alteration may prevent the formation of prominent discrete damage features, promoting instead the development of rock slumps and distributed erosion.

Southern slope damage domain

The dip direction of LSZ ranges from northeast to southeast in the southern slope damage domain. Here, tensile slope damage features, in the form of tension cracks and grabens, are oriented in an east-west direction, except for some north-trending counterscarps at the base of the slope. The tensile damage appears to be related to a prominent undulation in the LSZ, which causes the displacement direction at depth to differ between the north and the south parts of the domain, as evidenced by the borehole inclinometer logs (Fig. 18, Table 2). Westin (2017) observed that high rock mass damage exists at depth within the southern slope damage domain area, requiring installation of a shotcrete liner along the southern branch of Adit 1 (Fig. 18a). The location within the drainage adit where cracking of the shotcrete has been reported (BC Hydro 2009) appears to extend beyond the areas where surficial tensile damage is evident. This suggests that 1) increased tectonic damage may affect the rock mass in this area, or 2) internal damage and deformation may have occurred at depth without any obvious surficial evidence or that the evidence has been hidden beneath a cover of debris. Internal tensile slope damage likely resulted from normal faulting, which is reflected in cracks trending east-west and a graben in the upper part of the damage domain (Fig. 18b). The location of the north-trending counterscarps at the base of the slope is consistent with the low dip angle (<15°) of the lower shear zone in this domain and provides evidence of the internal damage and deformation in the Prandtl transition zone (Fig. 18c).

5.3. Evolution of the Downie Slide

Based on comparisons of slope damage features, the map of the LSZ, and displacement directions, we conclude that the style (tensile vs. shear), orientation, and distribution of surficial and internal slope damage features on the Downie Slide are related to: 1) displacement along a sliding surface with a complex geometry; and 2) rock mass damage associated with the Fissure Creek structure.

In general, the deformation and failure of rock slopes can be viewed as happening in three time-dependent stages: regressive, progressive, and post-failure (Dick et al. 2015). Stead and Eberhardt (2013) suggested that, as a slope deforms, slope damage progressively accumulates and at a rate dependent on the rate of movement of the slope. Slope damage initiates at the onset of failure, marking the passage from the regressive, or steady-state, stage to the progressive stage, which is characterized by an acceleration of movement and significant deformation and weakening of slope materials (Dick et al. 2015) (Fig. 19). The rate of displacement and accumulation of slope damage then decrease rapidly, and a post-failure condition is reached.

Such a conceptual model can be used to interpret the evolution of the Downie Slide (Table 4). In order to infer the deformation stage that presently characterizes the Downie Slide, we provide a brief analysis and discussion of present and past displacement rates at depth. Prior to the installation of the drainage system, displacement rates up to 10 mm/year were observed on the LSZ (BC Hydro 2010). These rates of displacement are not sufficient to account for the estimated 300 m of total displacement over the up to 10,000 years that the Downie Slide has existed. We thus

conclude that the displacement rates in the past have been substantially greater than the pre- and post-drainage values and that the Downie Slide is currently in the post-failure stage. In our conceptual model for the Downie Slide, the formation and development of slope damage occurred mainly near the end of the progressive stage, at the end of which the maximum displacement rates were achieved. The onset of failure probably happened during or shortly after deglaciation due to river erosion and oversteepening of the toe of the slope, removal of confining glacier ice, and high pore-water pressures (Kjelland 2004). The destabilizing effects of these processes are well known and can be observed at many sites in alpine environments (Leith, 2012; Kos et al. 2016; Clayton et al. 2017). The Downie Slide never blocked the Columbia River (Stantec 2009), thus even peak displacement rates were too low to cause the Downie Slide to transform into a rapid landslide. The upper distributed slope damage domain is characterized, as previously noted, by a topography significantly different from that of the rest of the slide area, suggesting that the mechanism and style of displacement there was different from the lower slope, as Kalenchuk et al. (2013) noted. The slide headscarp probably retrogressed during the stage of maximum displacement, driven by the progressive sliding of material away from the base of the headscarp and the subsequent lack of confinement, a positive feedback process. Thus, in view of the slow displacement rates that characterize the post-failure stage, present-day instabilities along the west cliff are likely to be limited to small, structurally controlled failures.

6 Conclusions

Lithology, geological structures, and geomorphology influence the nature, distribution, and orientation of slope damage that develops during the evolution of large slow-moving landslides. Investigations of slope damage using ALS, boreholes, and remote sensing datasets provide important insights into the spatial and temporal deformation of rock slopes.

We investigated the Downie Slide using ALS, digital photogrammetry, borehole logs, borehole inclinometer records, and GIS maps. An ALS dataset was used to document surficial slope damage and to define damage domains based on similar slope behavior and deformation features. Digital photogrammetric techniques and laser scanning were employed to characterize the rock mass and perform discontinuity mapping inside a drainage adit and along the headscarp. We reconstructed the geometries of two shear zones from borehole core logs and borehole inclinometer records using a kriging approach, and further analyzed them in a GIS environment.

We note a strong relationship between the orientation of the reconstructed lower shear zone (LSZ) and displacement azimuths at depth recorded by borehole inclinometers. The LSZ is characterized by a multi-planar morphology, and the spatial distribution, orientation, and types of surficial slope damage features mapped using the ALS dataset differ throughout the slide area as a function of the changes in the dip direction of the LSZ. Our GIS analysis also allowed us to identify a previously unrecognized, large, east-west trending structure co-linear with part of the Fissure Creek valley west of the slide. This structure intersects the slide, appears to control the morphology of the LSZ, and influences the geometry of retrogression of the landslide. The intersection of the Fissure Creek

structure with a Prandtl transition zone near the toe of the slide created a concentration of damage with associated faster and greater displacements, higher surface roughness, and enhanced erosion. These findings show that geological structures can be a major factor controlling slope deformation and thus the evolution, type, and spatial distribution of both internal and surficial slope damage.

Finally, we present a new conceptual model for the evolution of the Downie Slide. We note that the pre-drainage displacement rates cannot account for the estimated total displacement of the landslide, and thus significantly higher rates occurred in the past. We suggest that: 1) the Downie Slide initiated soon after deglaciation and is currently in a post-failure condition; 2) most observed slope damage features formed during the progressive stage of the failure when displacement rates were much higher than today; 3) retrogression of the landslide coincided with, and resulted from, downward displacement of the lower blocks due to a lack of confinement (a self-feeding process started that led to the progressive westward extension of the hummocky region in the upper slope); and 4) under present-day climatic conditions, deformation rates in the post-failure stage of evolution of the Downie Slide are unlikely to change from the creep rates currently being measured on this extensively instrumented slope.

The following work would further improve understanding of the factors controlling slope deformation and slope damage at the Downie Slide: 1) collection of subsurface data in those parts of the slide where the morphology of the shear zones is poorly constrained, such as the upper slope (i.e., upper distributed damage domain) and near the slide boundaries; 2) detailed structural analyses within the slide and along the Fissure Creek structure to investigate the relationships between regional structural geology and shear zone geometry; and 3) conceptual numerical modelling to verify and highlight the role of structural geology, lithology, and shear zone morphology on the location, orientation, and spatial distribution of slope damage across the slide.

Author contributions. Conceptualization: Davide Donati, Allison M. Westin, Doug Stead, John J. Clague, Thomas W. Stewart. Methodology: Davide Donati, Allison Westin, Doug Stead, John J. Clague. Formal analysis and investigation: Davide Donati, Allison M. Westin. Writing of original draft: Davide Donati. Review and editing: Allison M. Westin, Doug Stead, John J. Clague, Thomas W. Stewart, Martin S. Lawrence, Julia Marsh. Funding: Doug Stead. Supervision: Doug Stead; John J. Clague, Thomas W. Stewart, Martin S. Lawrence.

Acknowledgments. The authors thank BC Hydro and Power Authority for granting and facilitating access to the site and for providing access to its topographic, geological, and monitoring database of the Downie Slide; Chris Bray for flying the UAV at the site; and Emre Onsel, Koeben Jurykovsky, Ryan Kremsater, and Taylor Piller for assistance in the field. Two anonymous reviewers provided feedback that improved the quality of the paper.

References

Adhikary DP, Dyskin AV, Jewell RJ, Stewart DP (1997) A study of the mechanism of flexural toppling failure of rock slopes. Rock Mech Rock Eng 30:75–93. doi:10.1007/BF01020126

Agliardi F, Crosta GB, Frattini P, Malusà MG (2013a) Giant non-catastrophic landslides and the long-term exhumation of the European Alps. Earth Planet Sci Lett 365:263–274. doi:10.1016/j.epsl.2013.01.030

Agliardi F, Crosta GB, Meloni F, Valle, C, Rivolta C et al (2013b) Structurally-controlled instability, damage and slope failure in a porphyry rock mass. Tectonophysics 605:34–47. doi:10.1016/j.tecto.2013.05.033

Agliardi F, Crosta G, Zanchi A (2001) Structural constraints on deep-seated slope deformation kinematics. Eng Geol 59:83–102. doi:10.1016/S0013-7952(00)00066-1

Badger, TC (2002) Fracturing within anticlines and its kinematic control on slope stability. Environ Eng Geosci 8:19–33. doi:10.2113/gseegeosci.8.1.19

BC Hydro (1974) Revelstoke Project. Downie Slide investigation. Summary of the 1973 exploration program. BC Hydro Power Authority Report 725. (Unpublished)

BC Hydro (1987) Downie Slide. BC Hydro Power Authority Report H1900. (Unpublished)

BC Hydro (2009) Downie Slide drainage improvements construction report. BC Hydro Power Authority Report E664. (Unpublished)

BC Hydro (2010) Downie Slide drainage improvement project. Stability reassessment. BC Hydro Power Authority Report E798. (Unpublished)

Benko B, Stead D (1998) The Frank Slide: A reexamination of the failure mechanism. Can Geotech J 35:299–311. doi:10.1139/cgj-35-2-299

Bolla A, Paronuzzi P (2020) Geomechanical field survey to identify an unstable rock slope: The Passo della Morte case history (NE Italy). Rock Mech Rock Eng 53:1521–1544. doi:10.1007/s00603-019-01963-w

Brown RL, Psutka JF (1980) Structural and stratigraphic setting of the Downie slide, Columbia River valley, British Columbia. Can J Earth Sci 17:698–709. doi:10.1139/e80-067

Chigira M (1992) Long-term gravitational deformation of rocks by mass rock creep. Eng Geol 32:157–184. doi:10.1016/0013-7952(92)90043-X

Chigira M, Hariyama T, Yamasaki S (2013) Development of deep-seated gravitational slope deformation on a shale dip-slope: Observations from high-quality drill cores. Tectonophysics 605:104–113. doi:10.1016/j.tecto.2013.04.019

Clayton A, Stead D, Kinakin D, Wolter A (2017) Engineering geomorphological interpretation of the Mitchell Creek landslide, British Columbia, Canada. Landslides 14:1655–1675. doi:10.1007/s10346-017-0811-1

CloudCompare [GPL software] (2019) Version 2.10 retrieved from http://www.cloudcompare.org/

Dick GJ, Eberhardt E, Cabrejo-Liévano AG, Stead D, Rose ND (2015) Development of an early-warning time-of-failure analysis methodology for open-pit mine slopes utilizing ground-based slope stability radar monitoring data. Can Geotech J 52(4):515–529. doi:10.1139/cgj-2014-0028

Donati D (2019) The characterization of slope damage using an integrated remote sensing-numerical modelling approach. PhD thesis, Simon Fraser University, Burnaby, BC

Donati D, Stead D, Elmo D, Borgatti L (2019) A preliminary investigation on the role of brittle fracture in the kinematics of the 2014 San Leo landslide. Geosciences 9:256. doi:10.3390/geosciences9060256

Donati D, Stead D, Stewart TW, Marsh J (2020) Numerical modelling of slope damage in large, slowly moving rockslides: Insights from the Downie Slide, British Columbia, Canada. Eng Geol 273:105693. doi:10.1016/j.enggeo.2020.105693

Eberhardt E, Willenberg H, Loew S, Maurer H (2001) Active rockslides in Switzerland - Understanding mechanisms and processes. In: Kuhne M. (ed), Landslides – Causes, Impacts and Countermeasures. Proceedings of the UEF International Conference on Landslides - Causes, Impacts and Countermeasures, 17-21 June, Davos, Switzerland, pp 25–34

Elmo D, Donati D, Stead D (2018) Challenges in the characterisation of intact rock bridges in rock slopes. Eng Geol 245:81–96. doi:10.1016/j.enggeo.2018.06.014

ESRI (2017) ArcGIS 10.5. www.esri.com

Evans SG, Clague JJ (1999) Rock avalanches on glaciers in the Coast and St. Elias Mountains, British Columbia. In: Slope Stability and Landslides. Proceedings of the 13th Annual Vancouver Geotechnical Society, 28 May, Vancouver, BC, pp 115–123

Faro Technologies (2015) Scene. www.Faro.com

Francioni M, Stead D, Clague JJ, Westin A (2018) Identification and analysis of large paleo-landslides at Mount Burnaby, British Columbia. Environ Eng Geosci 24:221–235. doi:10.2113/EEG-1955

Gischig VS, Eberhardt E, Moore JR, Hungr O (2015) On the seismic response of deep-seated rock slope instabilities — Insights from numerical modeling. Eng Geol 193:1–18. doi:10.1016/j.enggeo.2015.04.003

Glueer F, Loew S, Manconi A, Aaron J (2019) From toppling to sliding: progressive evolution of the Moosfluh Landslide, Switzerland. J Geophys Res: Earth Surf 124:2899–2919. doi:10.1029/2019JF005019

Golden Software (2016) Surfer 14. www.goldensoftware.com/products/surfer

Gschwind S, Loew S, Wolter A (2019) Multi-stage structural and kinematic analysis of a retrogressive rock slope instability complex (Preonzo, Switzerland). Eng Geol 252:27–42. doi:10.1016/j.enggeo.2019.02.018

Hobson RD (1972) Surface roughness in topography: Quantitative approach. In: Chorley RJ (ed), Spatial Analysis in Geomorphology. Harper and Row, New York, pp 221–245

Humair F, Pedrazzini A, Epard JL, Froese CR, Jaboyedoff M (2013) Structural characterization of turtle mountain anticline (Alberta, Canada) and impact on rock slope failure. Tectonophysics 605:133–148. doi:10.1016/j.tecto.2013.04.029

Hungr O, Leroueil S, Picarelli L (2014) The Varnes classification of landslide types, an update. Landslides 11:167–194. doi:10.1007/s10346-013-0436-y

Imrie AS, Moore DP, Enegren EG (1992) Performance and maintenance of the drainage system at Downie Slide. In: Bell DH (ed), Landslides: Proceedings of the Sixth International Symposium, 10-14 February, Christchurch, New Zealand, pp 751–757

InnovMetric (2019) Polyworks MS 19, IR 5. https://www.innovmetric.com/

Jaboyedoff M, Oppikofer T, Abellán A, Derron MH, Loye A, Metzger R, Pedrazzini A (2012) Use of LiDAR in landslide investigations: A review. Nat Hazards 61:5–28. doi: 10.1007/s11069-010-9634-2

Jaboyedoff M, Penna I, Pedrazzini A, Baroň I, Crosta GB (2013) An introductory review on gravitational-deformation induced structures, fabrics and modeling. Tectonophysics 605:1–13. doi:10.1016/j.tecto.2013.06.027

Kalenchuk KS, Diederichs MS, Hutchinson DJ (2012) Three-dimensional numerical simulations of the Downie Slide to test the influence of shear surface geometry and heterogeneous shear zone stiffness. Comp Geosci 16:21–38. doi:10.1007/s10596-011-9245-3

Kalenchuk KS, Hutchinson DJ, Diederichs MS (2009) Application of spatial prediction techniques to defining three-dimensional landslide shear surface geometry. Landslides 6:321–333. doi:10.1007/s10346-009-0168-1

Kalenchuk KS, Hutchinson DJ, Diederichs MS (2013) Geomechanical interpretation of the Downie Slide considering field data and three-dimensional numerical modelling. Landslides 10:737–756. doi: 10.1007/s10346-012-0363-3

Kemeny J (2003) The time-dependent reduction of sliding cohesion due to rock bridges along discontinuities: A fracture mechanics approach. Rock Mech Rock Eng 36:27–38. doi:10.1007/s00603-002-0032-2

Kjelland NH (2004) Slope stability analysis of Downie Slide: Numerical modelling and GIS data analysis for geotechnical decision support. MSc thesis, Queen's University, Kingston, ON

Kos A, Amann F, Strozzi T, Delaloye R, von Ruette J, Springman S (2016) Contemporary glacier retreat triggers a rapid landslide response, Great Aletsch Glacier, Switzerland. Geophys Res Lett 43:12,466–12,474. doi:10.1002/2016GL071708

Kvapil R, Clews M (1979) An examination of the Prandtl mechanism in large dimension slope failures. Trans Inst Min Metal Sect A 88:A1–A5

Leith KJ (2012) Stress development and geomechanical controls on the geomorphic evolution of alpine valleys. PhD thesis, ETH Zurich, Zurich, Switzerland

Lo CM, Feng ZY (2014) Deformation characteristics of slate slopes associated with morphology and creep. Eng Geol 178:132–154. doi:10.1016/j.enggeo.2014.06.011

Massey CI, Petley DN, McSaveney MJ (2013) Patterns of movement in reactivated landslides. Eng Geol 159:1–19. doi:10.1016/j.enggeo.2013.03.011

Massironi M, Zampieri D, Superchi L, Bistacchi A, Ravagnan R, Bergamo A, Ghirotti M, Genevois R (2013) Geological structures of the Vajont landslide. Ital J Eng Geol Environ 6:573–582. doi:10.4408/IJEGE.2013-06.B-55

Mencl V (1966) Mechanics of landslides with non-circular slip surfaces with special reference to the Vaiont Slide. Géotechnique 16:329–337. doi:10.1680/geot.1966.16.4.329

Moore D (1989) Panelist contribution, Downie slide and Dutchman's Ridge. In: Proceedings of the 12th International Conference on Soil Mechanics and Foundation Engineering, Rio de Janeiro, Brazil, 13-18 August, pp 3063-3065

Paronuzzi P, Bolla A (2015) Gravity-induced rock mass damage related to large en masse rockslides: Evidence from Vajont. Geomorphology 234:28–53. doi:10.1016/j.geomorph.2015.01.008

Petley D (2012) Global patterns of loss of life from landslides. Geology 40:927–930. doi:10.1130/G33217.1

Piteau DR, Mylrea FH, Blown IG (1978) Downie Slide, Columbia River, British Columbia, Canada. In: Voight B (ed), Rockslides and Avalanches, Volume 1. Elsevier Science, pp 365–392

Planet Team (2018) Planet application program interface: In Space for Life on Earth. San Francisco, CA. https://api.planet.com

Preisig G, Eberhardt E, Smithyman M, Preh A, Bonzanigo L (2016) Hydromechanical rock mass fatigue in deep-seated landslides accompanying seasonal variations in pore pressures. Rock Mech Rock Eng 49:2333–2351. doi:10.1007/s00603-016-0912-5

Read PB, Brown RL (1981) Columbia River fault zone: Southeastern margin of the Shuswap and Monashee complexes, southern British Columbia. Can J Earth Sci 18:1127–1145. doi:10.1139/e81-108

Roberti G, Ward B, van Wyk de Vries B, Friele P, Perotti L, Clague JJ, Giardino M (2018) Precursory slope distress prior to the 2010 Mount Meager landslide, British Columbia. Landslides 15:637–647. doi:10.1007/s10346-017-0901-0

Rocscience (2016). DIPS version 7. www.Rocscience.com

Sappington JM, Longshore KM, Thompson DB (2007) Quantifying landscape ruggedness for animal habitat analysis: A case study using bighorn sheep in the Mojave Desert. J Wildland Management 71:1419-1426. doi:10.2193/2005-723

Semenza E, Ghirotti M (2000) History of the 1963 Vaiont slide: The importance of geological factors. Bull Eng Geol Environ 59:87–97. doi:10.1007/s100640000067

Shea T, van Wyk de Vries B (2008) Structural analysis and analogue modeling of the kinematics and dynamics of rockslide avalanches. Geosphere 4:657-686. doi:10.1130/GES00131.1

Stantec (2009) Bedrock and surficial geology of Downie Slide, final report. Prepared for BC Hydro and Power Authority. (Unpublished)

Stead D, Eberhardt E (2013) Understanding the mechanics of large landslides. Ital J Eng Geol Environ - Book Ser 6:85–112. doi:10.4408/IJEGE.2013-06.B-07

Stead D, Wolter A (2015) A critical review of rock slope failure mechanisms: The importance of structural geology. J Struct Geol 74:1–23. doi:10.1016/j.jsg.2015.02.002

Sturzenegger M, Stead D (2009) Quantifying discontinuity orientation and persistence on high mountain rock slopes and large landslides using terrestrial remote sensing techniques. Nat Hazards Earth Syst Sci 9:267–287. doi:10.5194/nhess-9-267-2009

Westin AM (2017) Downie Slide: An integrated remote sensing approach to characterization of a very slow moving landslide. MSc thesis, Simon Fraser University, Burnaby, BC

Westoby MJ, Brasington J, Glasser NF, Hambreya MK, Reynoldsc JM (2012) "Structure-from-Motion" photogrammetry: A low-cost, effective tool for geoscience applications. Geomorphology 179:300–314. doi:10.1016/j.geomorph.2012.08.021

Wolter A, Gischig V, Stead D, Clague JJ (2016a) Investigation of geomorphic and seismic effects on the 1959 Madison Canyon, Montana, landslide using an integrated field, engineering geomorphology mapping, and numerical modelling approach. Rock Mech Rock Eng 49:2479–2501. doi:10.1007/s00603-015-0889-5

Wolter A, Stead D, Ward BC, Clague JJ, Ghirotti M (2016b) Engineering geomorphological characterisation of the Vajont Slide, Italy, and a new interpretation of the chronology and evolution of the landslide. Landslides 13:1067-1081. doi:10.1007/s10346-015-0668-0

A reinterpretation of the Downie Slide (British Columbia, Canada) based on slope damage characterization and subsurface data interpretation

Davide Donati[1]* (ORCiD: 0000-0003-4083-5910); Allison M. Westin[2] (ORCiD: 0000-0001-6378-8550); Doug Stead[1]; John J. Clague[1]; Thomas W. Stewart[3]; Martin S. Lawrence[4]; Julia Marsh[3]

5 Simon Fraser University, Department of Earth Sciences, Burnaby, British Columbia, Canada

6 Provincial Agricultural Land Commission, Burnaby, British Columbia, Canada

7 BC Hydro and Power Authority, Vernon, British Columbia, Canada

8 BC Hydro and Power Authority, Burnaby, British Columbia, Canada

* Corresponding author: Davide Donati, email: davide_donati@sfu.ca

Figures and tables follow

Figures

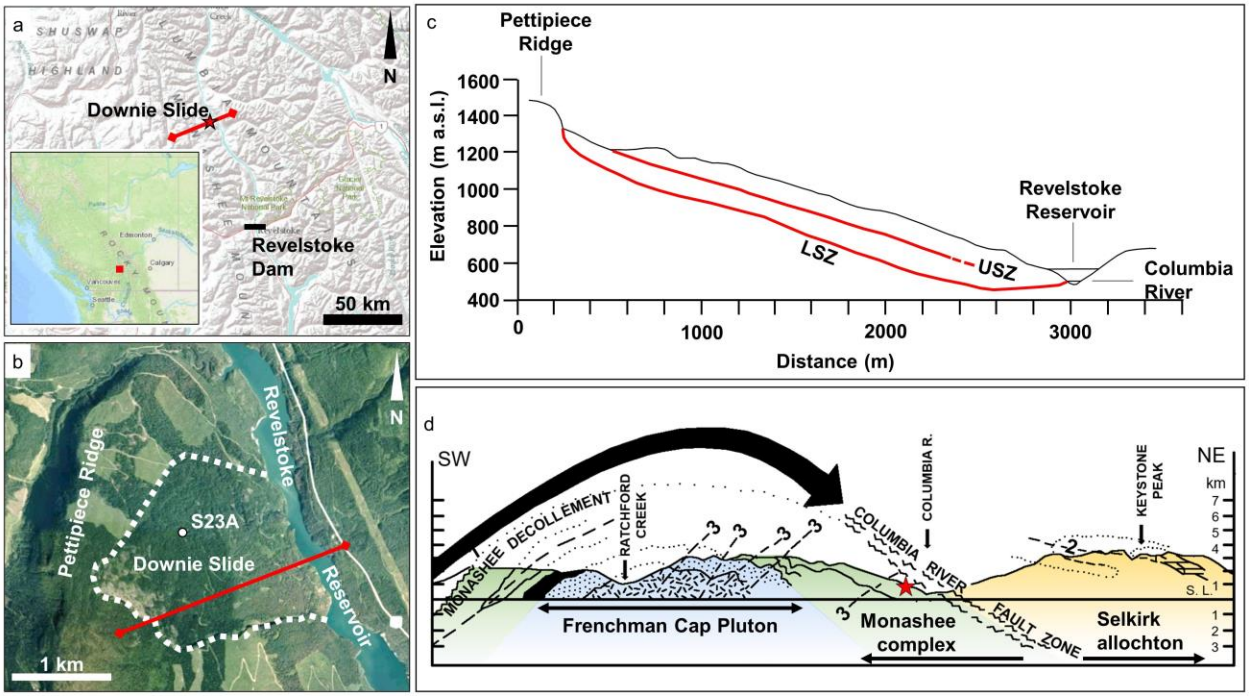

Fig. 1 **Overview of Downie Slide . a: Geographic overview (base maps from the US Geological Survey and Natural Resources Canada). The star indicates the location of the Downie Slide. The location of Revelstoke Dam is also shown. The red line identifies the geological section shown in panel c. b: 2003 satellite image of the Downie Slide (from Google Earth). White circle marks the location of borehole S23A shown in Fig. 2. Dotted line outlines the slide area. The red line identifies the location of the section shown in c. c: Geological section through the Downie Slide, showing the interpreted location of the LSZ and USZ. The elevation of the Columbia River prior to the reservoir impoundment is also shown (redrawn from Moore 1989). d: Geological section through the study area and the Downie Slide. Note the interpreted overthrust of the Selkirk Allochton along the Monashee Decollment, the Frenchman Cap Pluton intruding the Monashee Complex, and the inferred width of the Columbia River Fault Zone. Numbers 2 and 3 mark fold axes of tectonic deformation phases (modified from Read and Brown 1981). [2 column figure]**

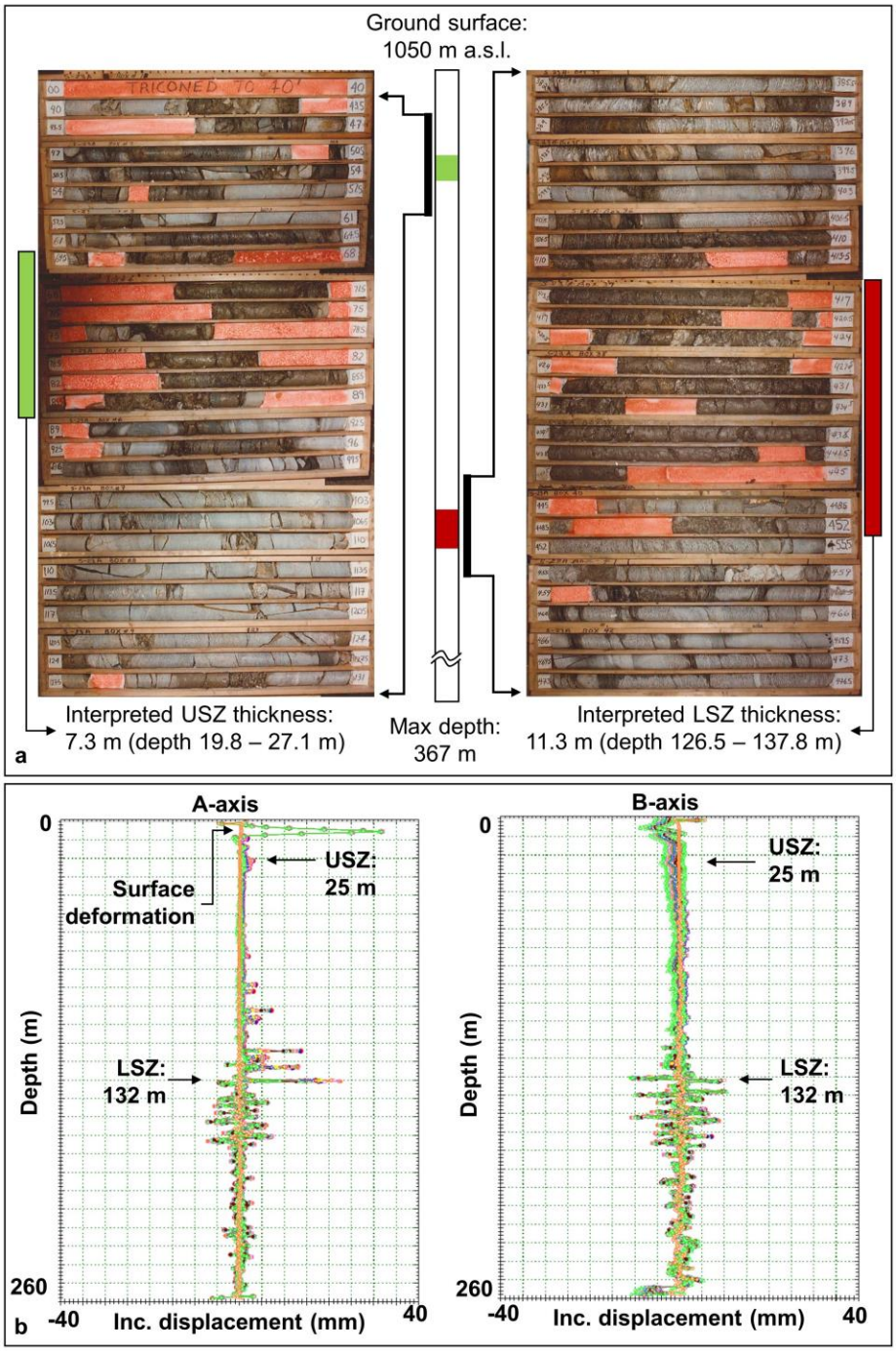

Fig. 2 **Core and an inclinometer log from borehole S23A, located in the central part of the Downie Slide (see Fig. 1 for location). a: Photographs of core and simplified log. Note the difference between the damaged, sheared, and altered rock mass forming the USZ and LSZ, and the less damaged rock mass outside the shear zones. The orange-brown coloured gaps in the photographs represent rock that was too weak or closely fractured (i.e., sheared) and was consequently not recovered during drilling. b: Incremental inclinometer log plot showing the location of the LSZ and USZ. Displacements at depth occur along a thin layer within a thick shear zone. Surficial deformation is also evident at this location, which is of limited significance for the overall slope behavior. [1.5 or 2 column figure]**

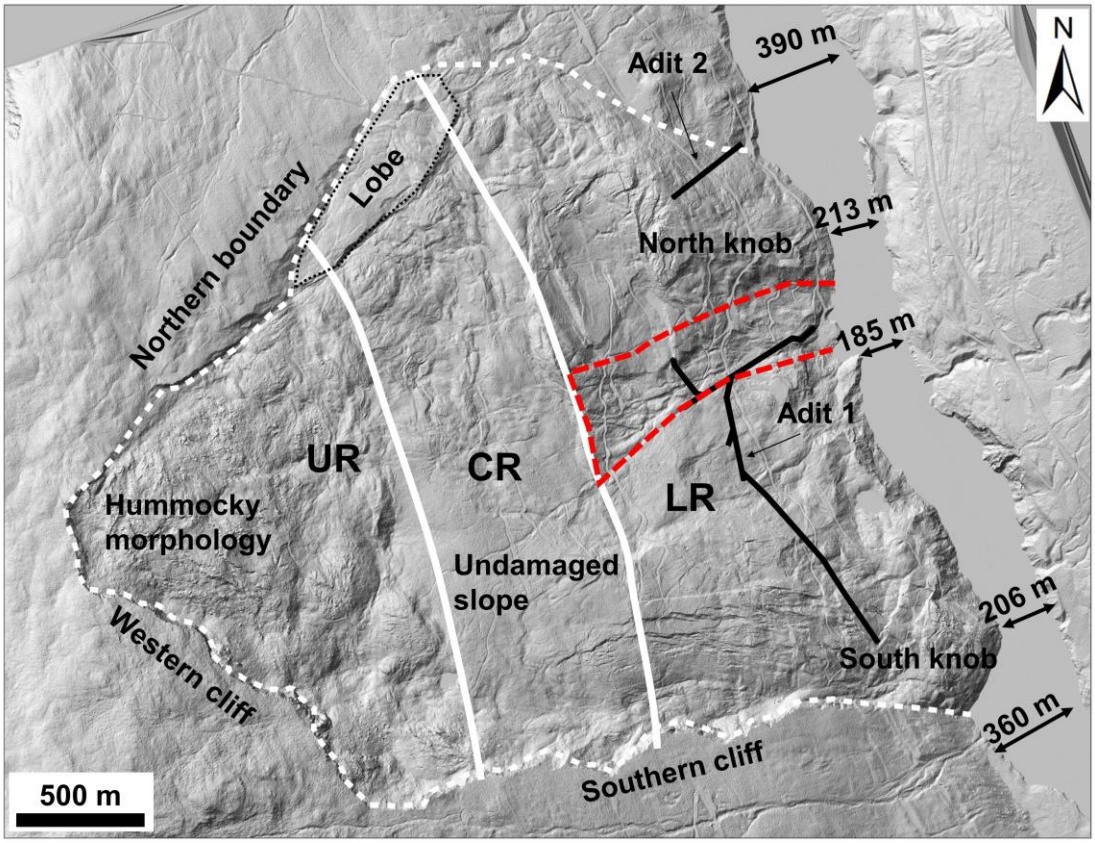

Fig. 3 **Geomorphic and hydrogeological overview of the Downie Slide area. Background image is the 2009 hillshade map of the Downie Slide (courtesy of BC Hydro). The dashed white line delineates the outer boundary of the slide. The dashed red line outlines the most actively deforming area of the slide. The solid black lines show the locations of the drainage adits. Note the differences in slope morphology between the hummocky upper slope, the undamaged central slope, the damaged surfaces of the North and South knobs, and constrictions in the reservoir due to the slide protruding into the valley. Solid white lines mark the boundaries of different hydrogeological domains within the slide area. UR: upper region; CR: central region; LR: lower region. [1 column figure]**

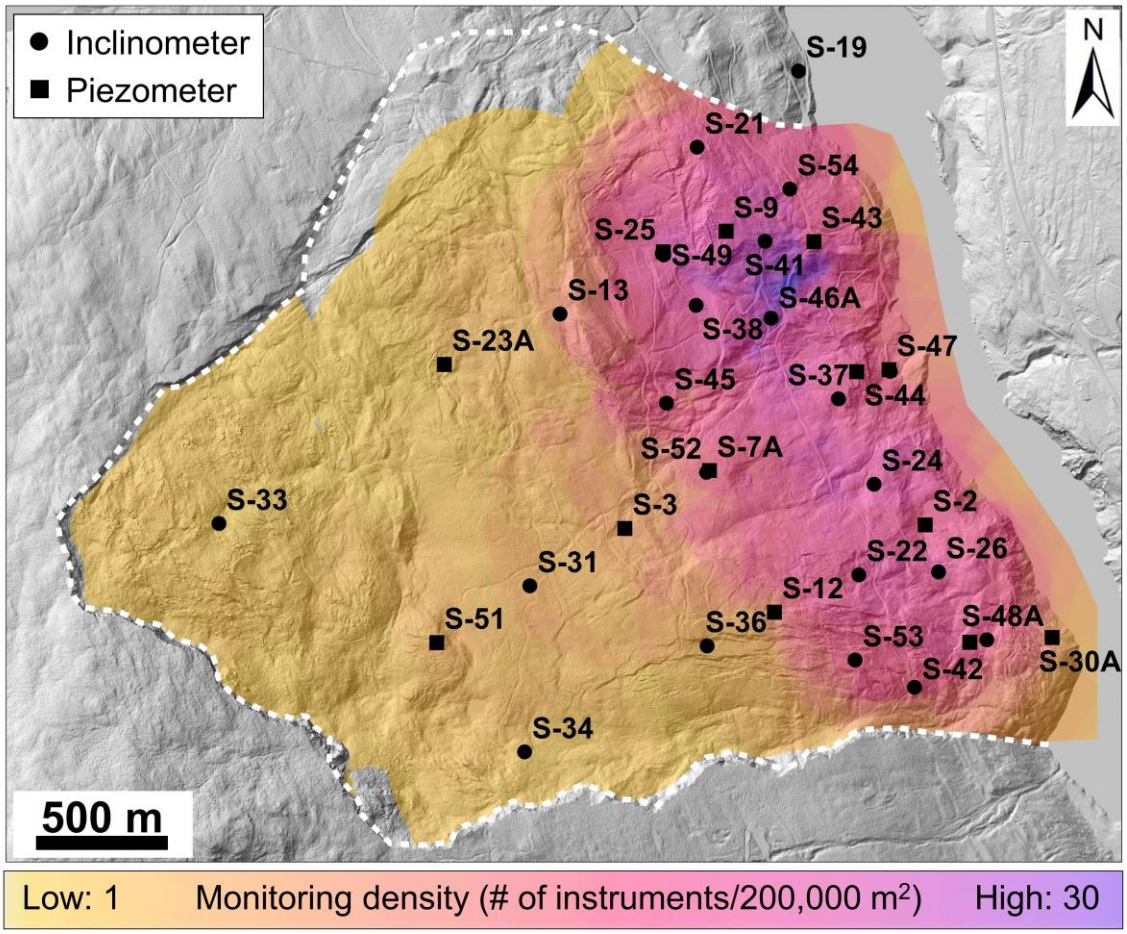

Fig. 4 **Monitoring system at the Downie Slide, showing the location of intrumented boreholes and the spatial density of monitoring instruments (computed as the number of instruments in a 250-m radius circle, using the "data metric" method in Surfer, Golden Software 2016). Multiple piezometers are generally installed in a single borehole. The dashed white line marks the outer limit of the slide. [1 or 1.5 column figure]**

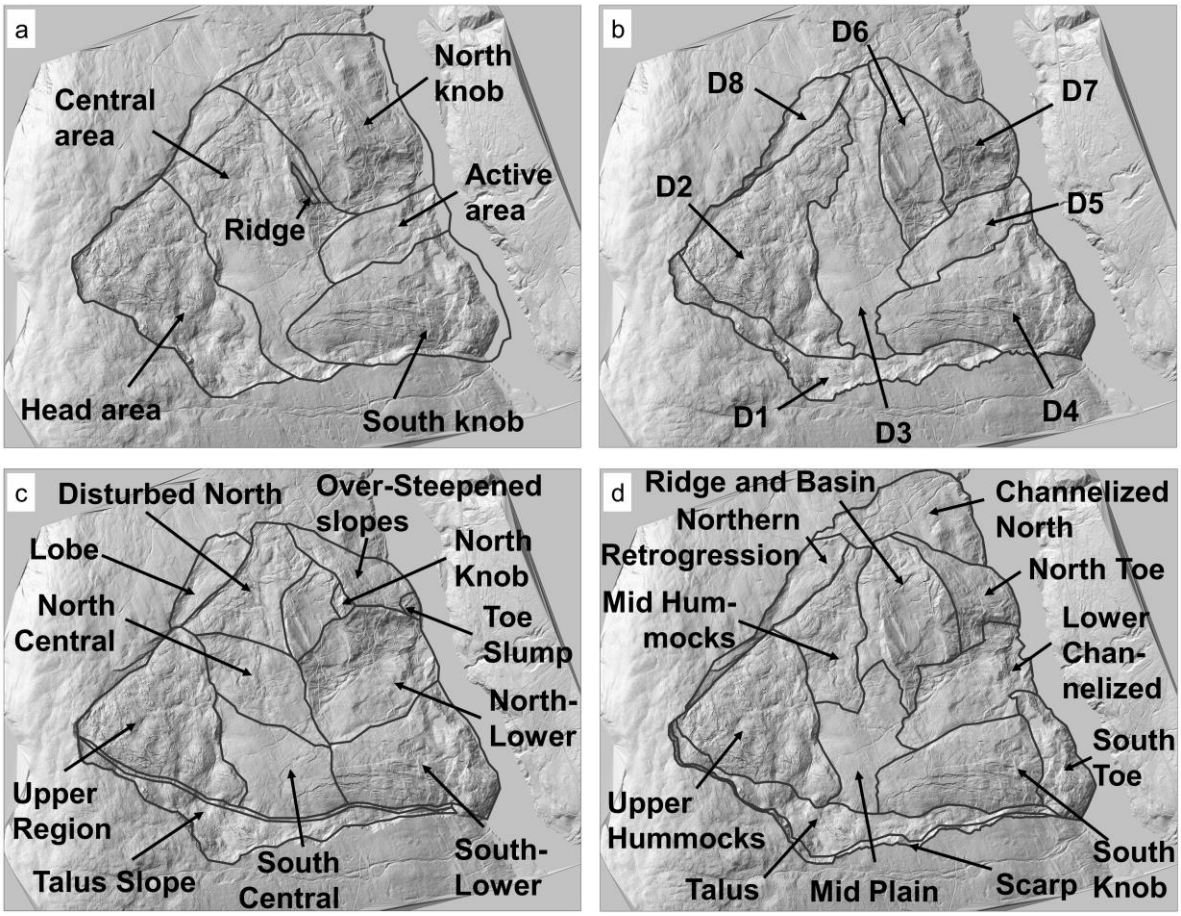

Fig. 5 **Summary of the landslide domains proposed for the Downie Slide. a: Piteau et al. (1978). b: Stantec (2009). c: Kalenchuk et al. (2013). d: Westin (2017). [2 column figure]**

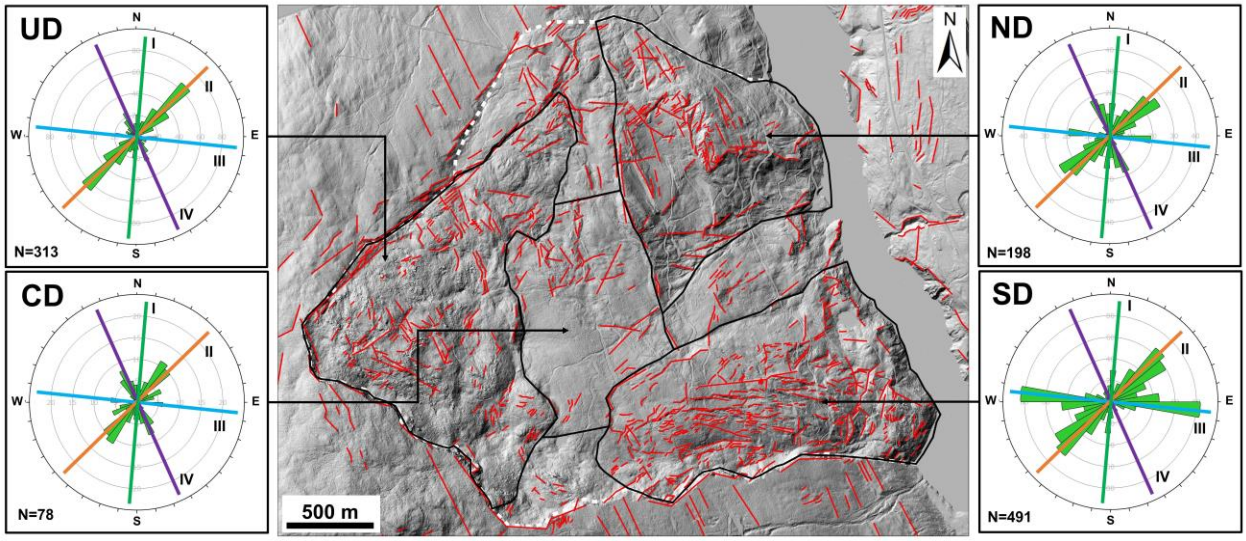

Fig. 6 **Slope damage domains identified within the Downie Slide. For each domain, the principal orientation trends of slope damage features are summarized in rosette diagrams, and the orientations of the trends I-IV are highlighted. UD: upper distributed slope damage domain. CD: central undamaged domain. ND: northern slope damage domain. SD: southern slope damage domain. [2 column figure]**

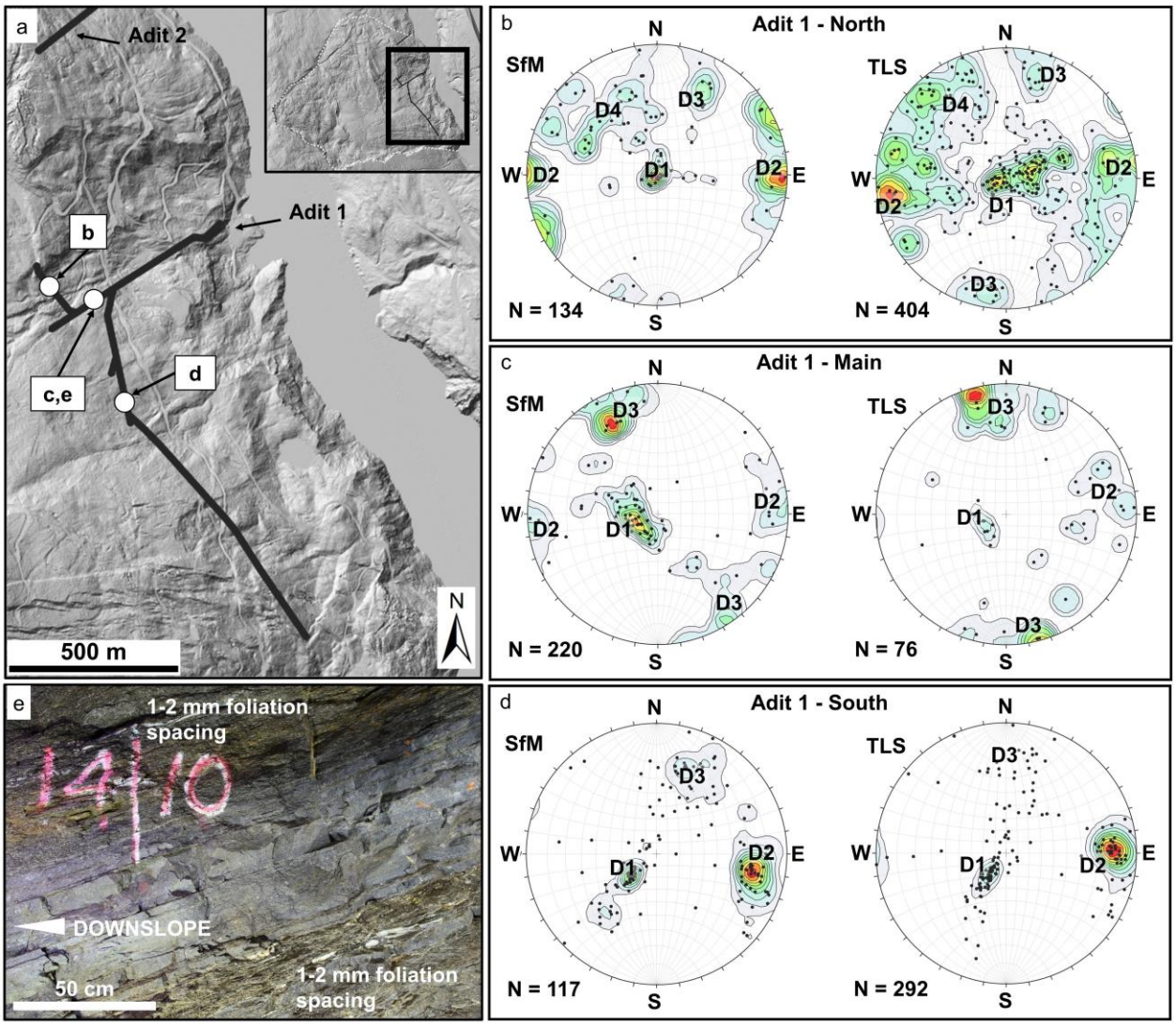

Fig. 7 **Underground rock mass characterization at the Downie Slide. a: Location of the investigated sections of Adit 1. b, c, d: SfM- and TLS-based stereonets of discontinuities mapped in, respectively, the northern, central, and southern branches of the drainage Adit 1. Terzaghi correction has been applied in the pole density contouring based on tunnel wall orientations. e: Example of rock mass characteristics in the drainage adits. Note alternation between closely foliated mica schist and higher quality quartz-feldspar gneiss. [1.5 or 2 column figure]**

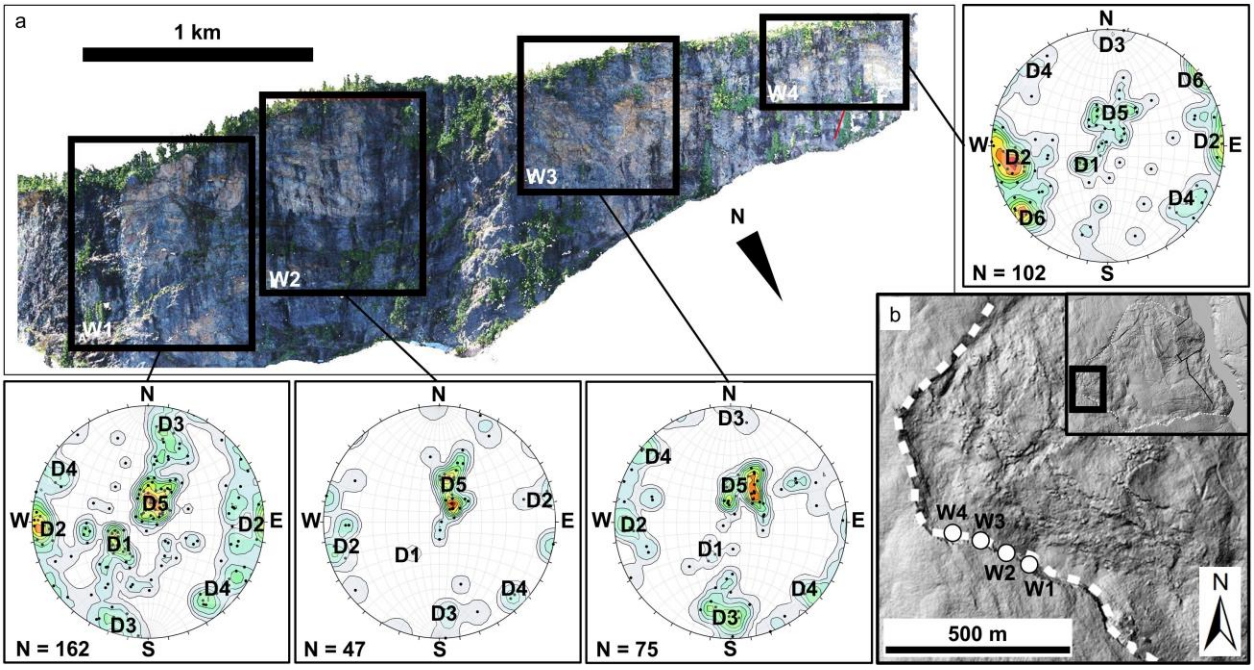

Fig. 8 **Summary of headscarp SfM window discontinuity mapping. a: Orthorectified photograph of part of the western headscarp showing the locations of windows W1-W4. The stereonet with the interpreted discontinuity sets is shown for each window. b: Locations of the windows in the ALS hillshade. Location within the Downie Slide is shown in the inset. [2 column figure]**

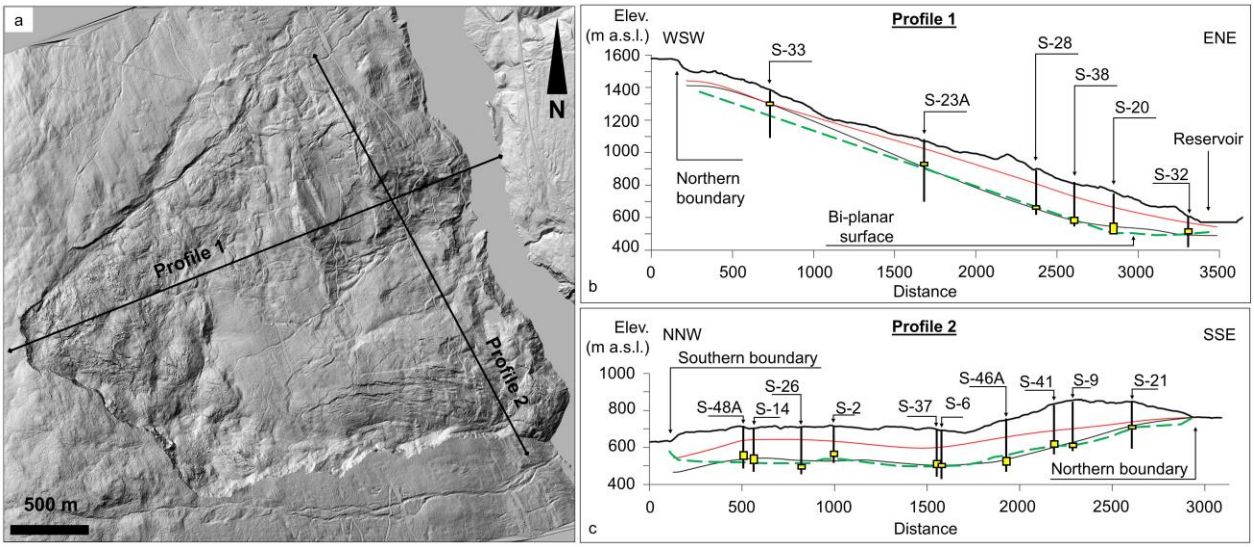

Fig. 9 **Geological cross-sections showing locations of the shear zones reconstructed in this study and comparison of the inferred position of the LSZ with its position identified in previous studies (BC Hydro 2010). a: Location of the sections within the Downie Slide. b: Profile 1. c: Profile 2. The vertical black lines mark the location and length of boreholes projected onto sections. The interpreted depth and thickness of the LSZ are represented by yellow bars. The LSZ and USZ are displayed in the sections as red and black lines, respectively. The dashed green line marks the LSZ as interpreted by BC Hydro (2010). Note the multi-planar configuration of the LSZ in profile 1 and the depth of the shear zones below the southern boundary in profile 2. [2 column figure]**

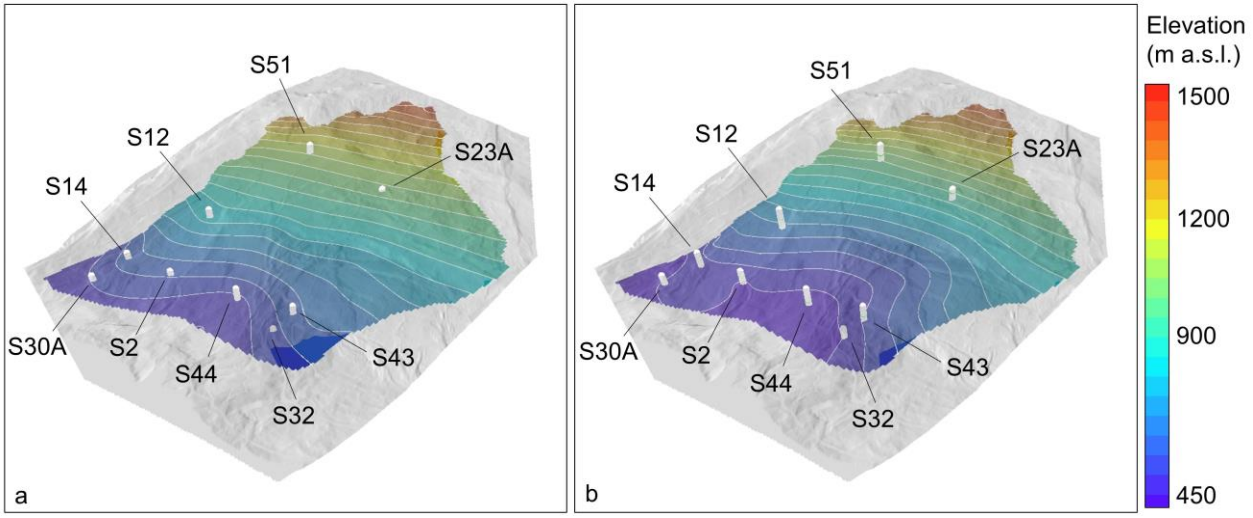

Fig. 10 **3D view of the reconstructed (a) USZ and (b) LSZ surfaces. Locations of the inclinometers included in Table 2 are shown. [2 column figure]**

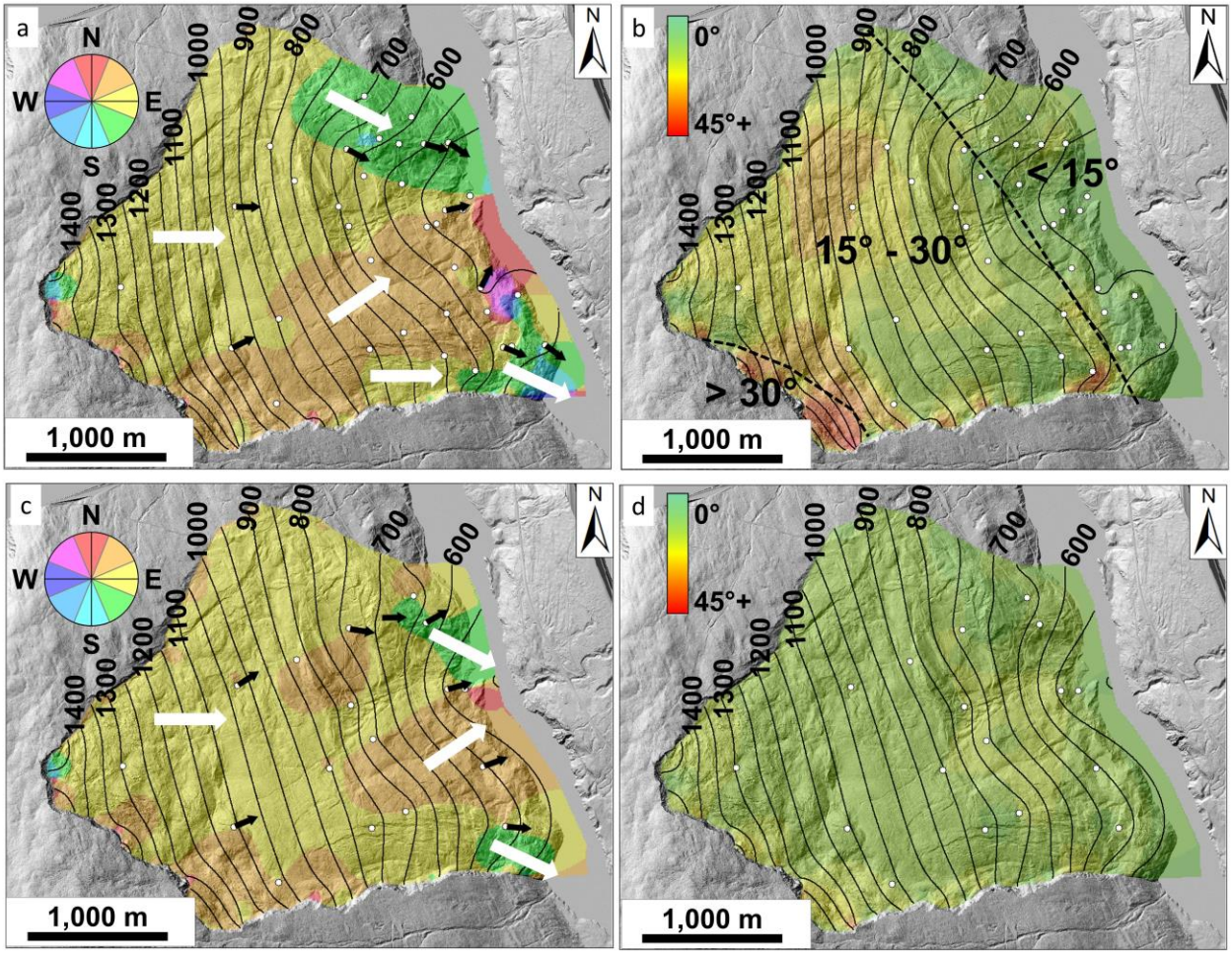

Fig. 11 **Morphology of the lower and upper shear zones. a: Aspect map showing the dip direction of the LSZ. White circles show the locations of boreholes used in the surface interpolation. Note the general agreement with the borehole inclinometer displacement directions (black arrows). b: Slope map showing changes in the gradient of the LSZ throughout the slide. Note the decrease in steepness of the LSZ towards the base of the slope. These maps highlight the multi-planar morphology of the LSZ. c: Aspect map of the USZ. d: Slope map of the USZ. White arrows in a and c are plotted for clarity and show the approximate dip direction of the LSZ. Black lines are contours on the base of each shear zone in metres a.s.l. [2 column figure]**

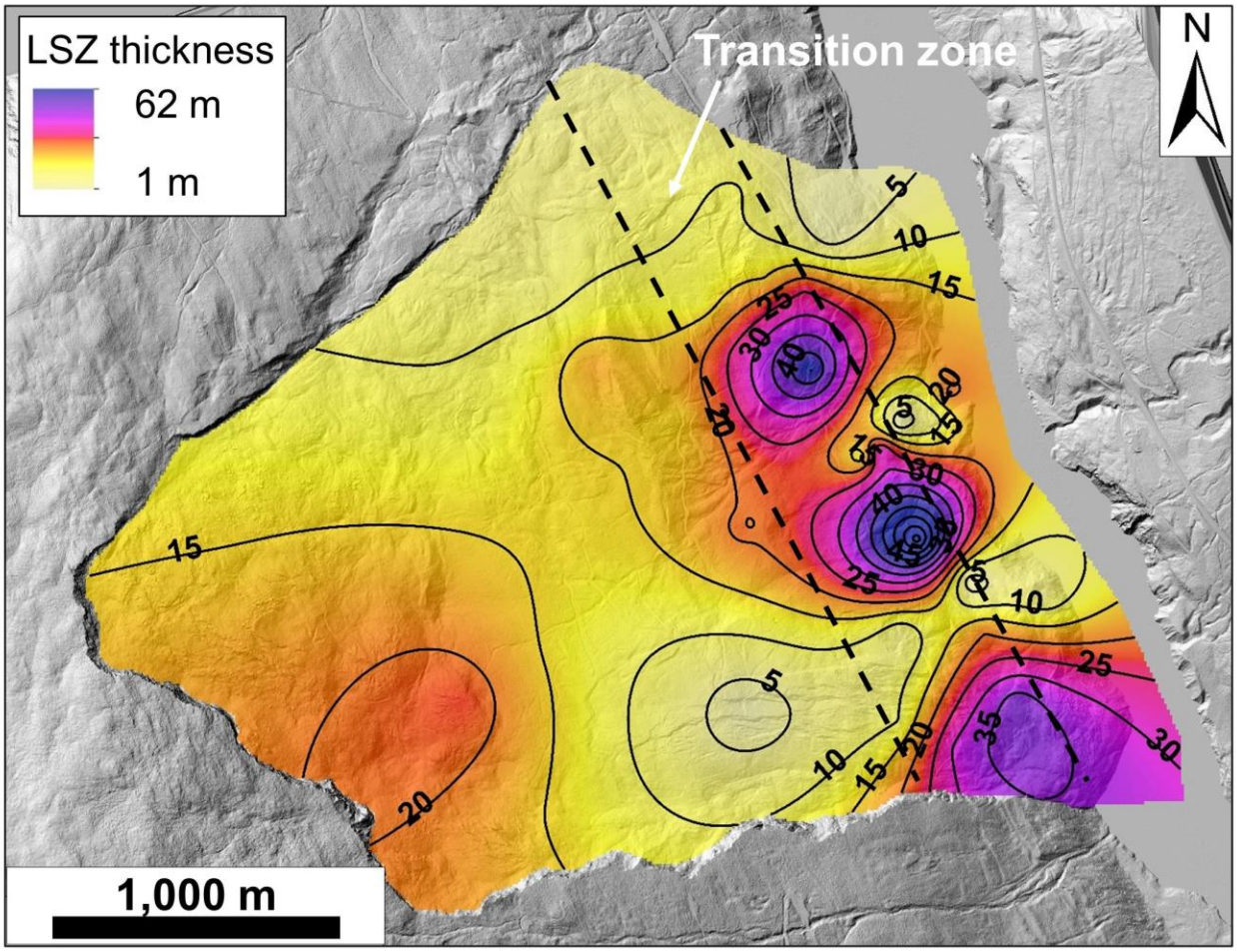

Fig. 12 **Map showing the thickness of the LSZ. Note the thickening of the shear zone beneath the lower slope. Dashed black lines show the inferred extent of the transition zone based on the change in gradient of the LSZ. [1 or 1.5 column figure]**

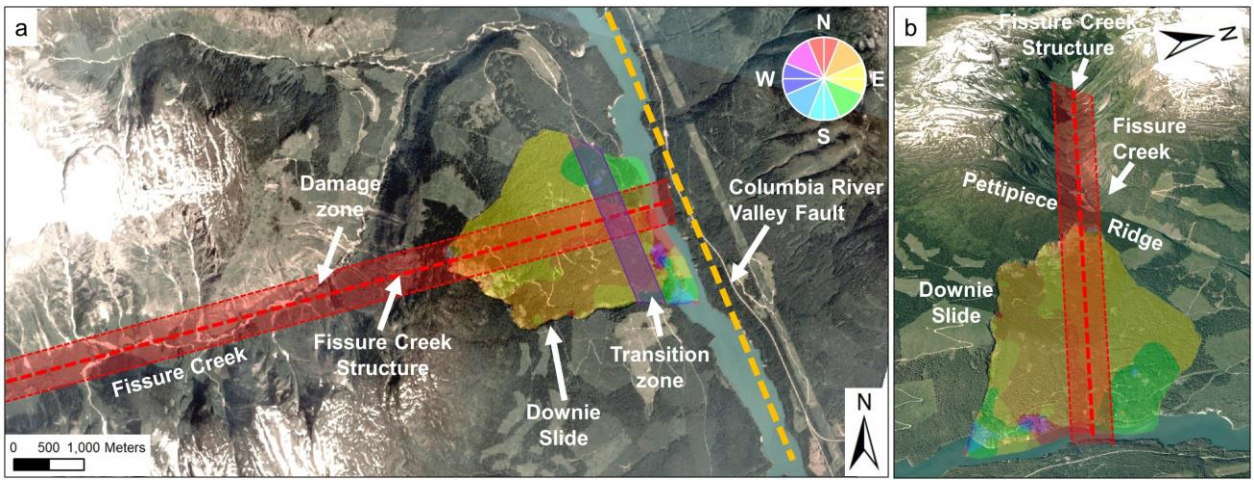

Fig. 13 **Relationship between slope damage and structural geology. a: Satellite image of the Downie Slide and surrounding area (image from Planet Team 2018). b: Oblique view from Google Earth. Note the alignment between Fissure Creek behind the Downie slide headscarp, the intersection of east- and northeast-dipping planes forming the LSZ (particularly in the central and lower slope), and the notch within the headscarp. [2 column figure]**

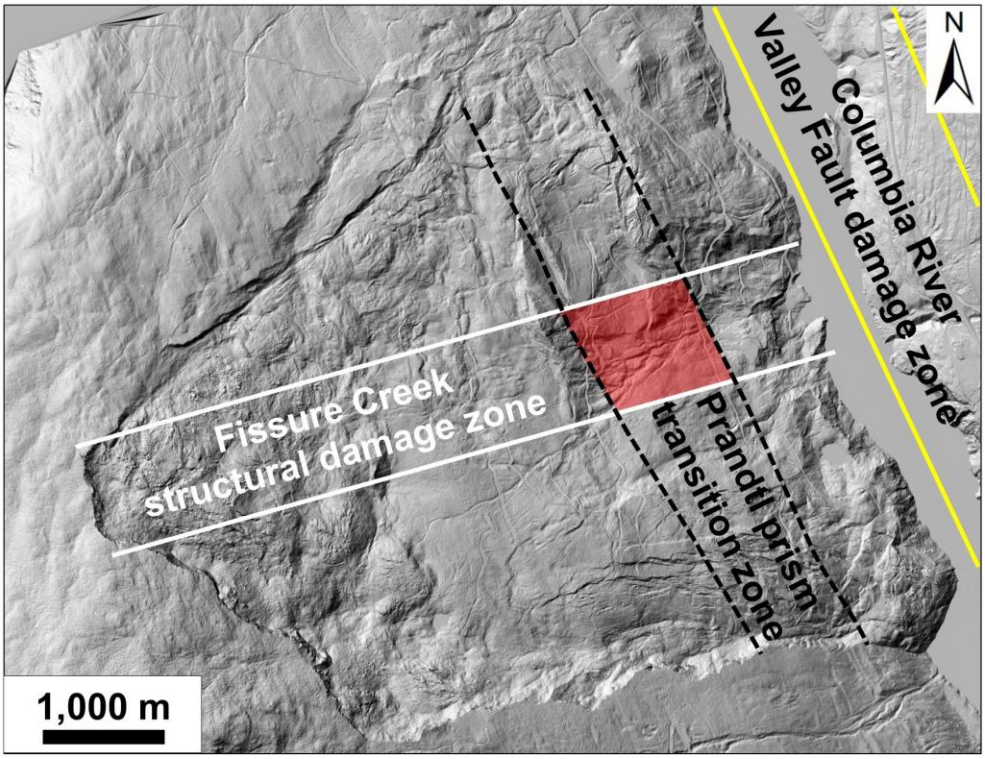

Fig. 14 **Conceptual internal slope damage distribution at the Downie Slide site. Solid and dashed lines bound inferred zones of structural and internal slope damage, respectively. The red highlighted area is the area of potential damage concentration at the intersection between the inferred Prandtl prism transition zone and the Fissure Creek structural damage zone. The damage zone of the Columbia River Fault (not to scale) is represented by the yellow lines. Note the correspondence between the damage zone area and the active slope displacement area within the lower slope (Fig. 3). [1 or 1.5 column figure]**

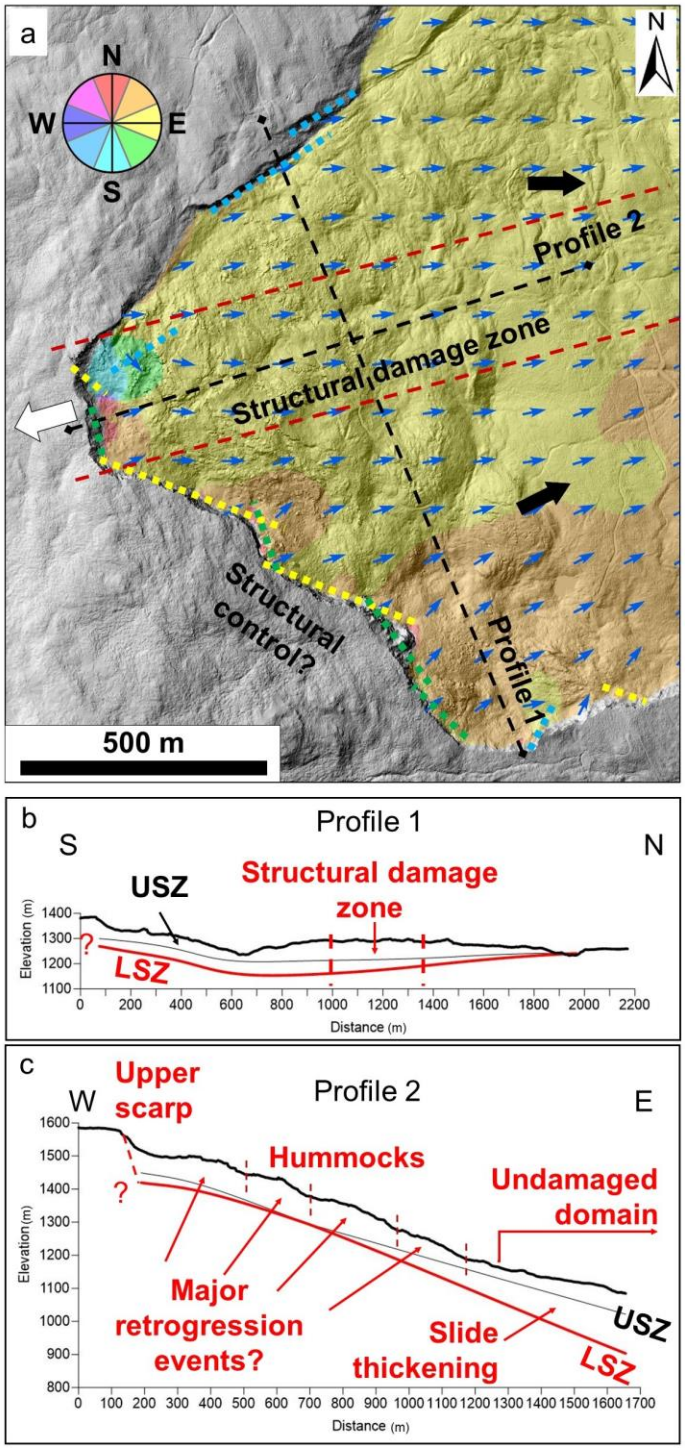

Fig. 15 **Interpretation of slope damage within the upper distributed slope damage domain. a: GIS aspect map. Blue arrows show the dip direction of the LSZ, and black arrows show the displacement direction in the borehole inclinometers along the shear zone. Dashed red lines bound the Fissure Creek structural damage zone. Dotted lines highlight linear structures that form the headscarp (similar colors indicate a similar orientation). b, c: Conceptual profiles through the domain. LSZ: lower shear zone; USZ: upper shear zone. [1.5 or 2 column figure]**

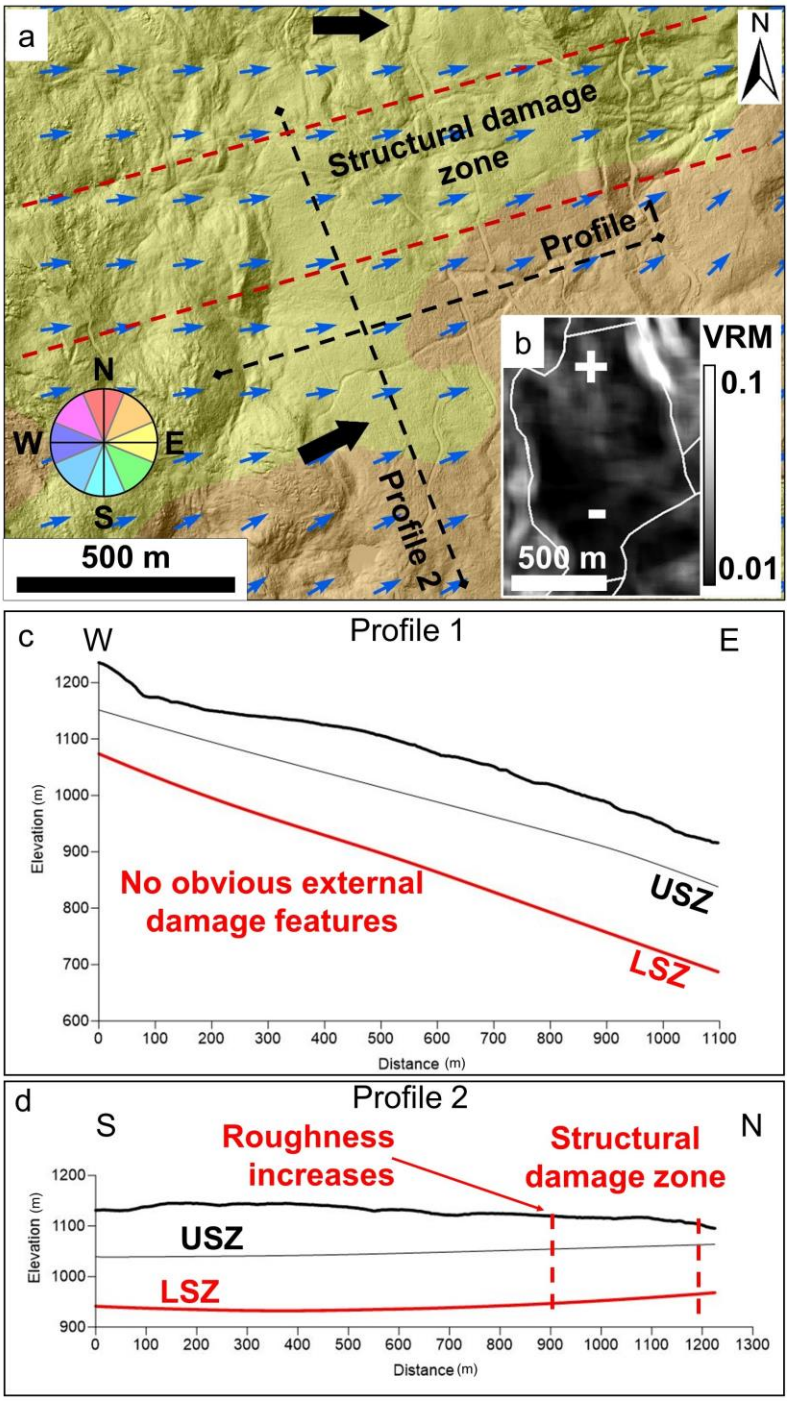

Fig. 16 **Interpretation of slope damage within the central undamaged domain. a: GIS aspect map overlain on the hillshade map. Blue arrows show the dip direction of the LSZ, and black arrows show the displacement direction in the borehole inclinometers at the LSZ. The dashed red lines bound the Fissure Creek damage zone that crosses the slide area. Note the absence of obvious external slope damage features. b: VRM map of the central undamaged domain (cfr. Fig. 2), showing an increase in surface roughness in the northern sector (+) compared to the southern sector (-). c, d: Conceptual sections through the domain. LSZ: lower shear zone; USZ: upper shear zone. [1.5 or 2 column figure]**

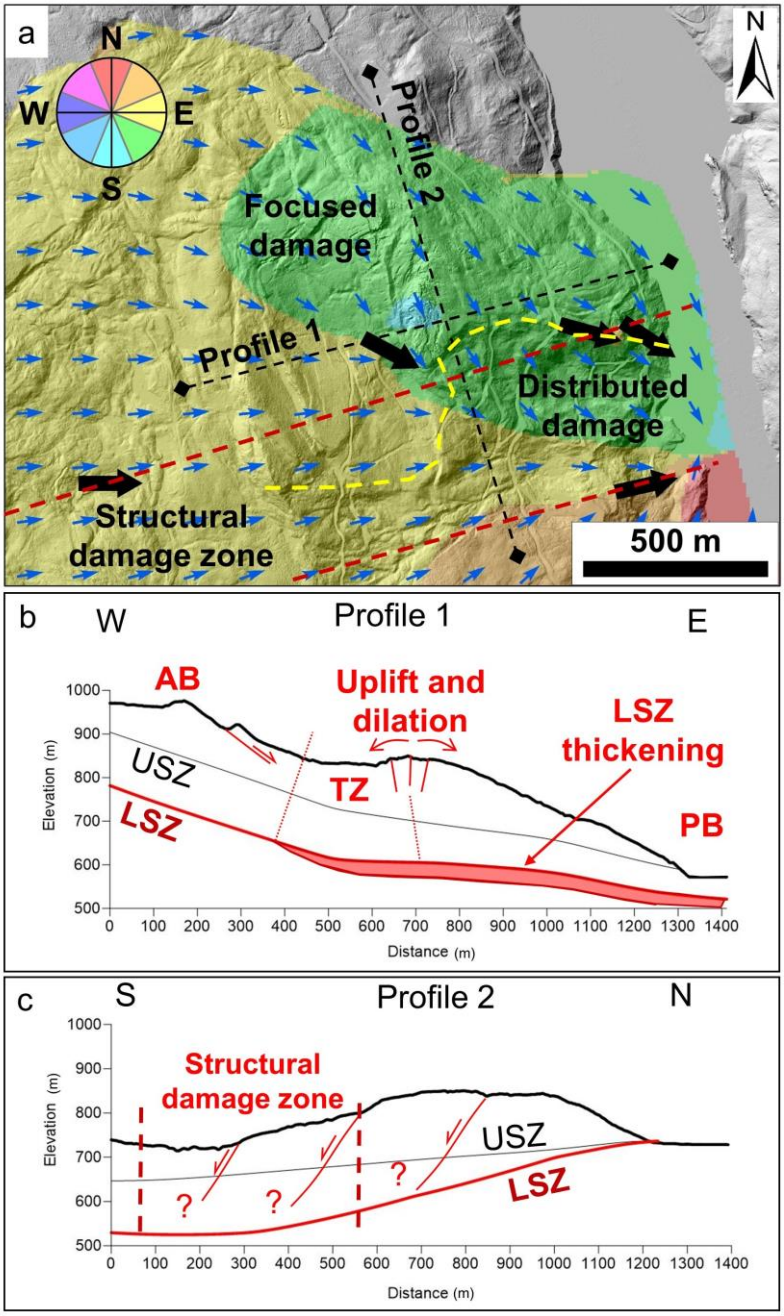

Fig. 17 **Interpretation of slope damage within the northern slope damage domain. a: GIS aspect map overlain on the hillshade map. Blue arrows show dip direction of the LSZ, and black arrows show the displacement direction in the inclinometers at the LSZ. The dashed yellow line is the boundary marking a southerly increase in distributed slope damage. The dashed red lines bound the Fissure Creek structural damage zone. b, c: Conceptual sections through the domain. LSZ: lower shear zone; USZ: upper shear zone; AB: active block; PB: passive block; TZ: transition zone (bounded by dotted red lines). [1.5 or 2 column figure]**

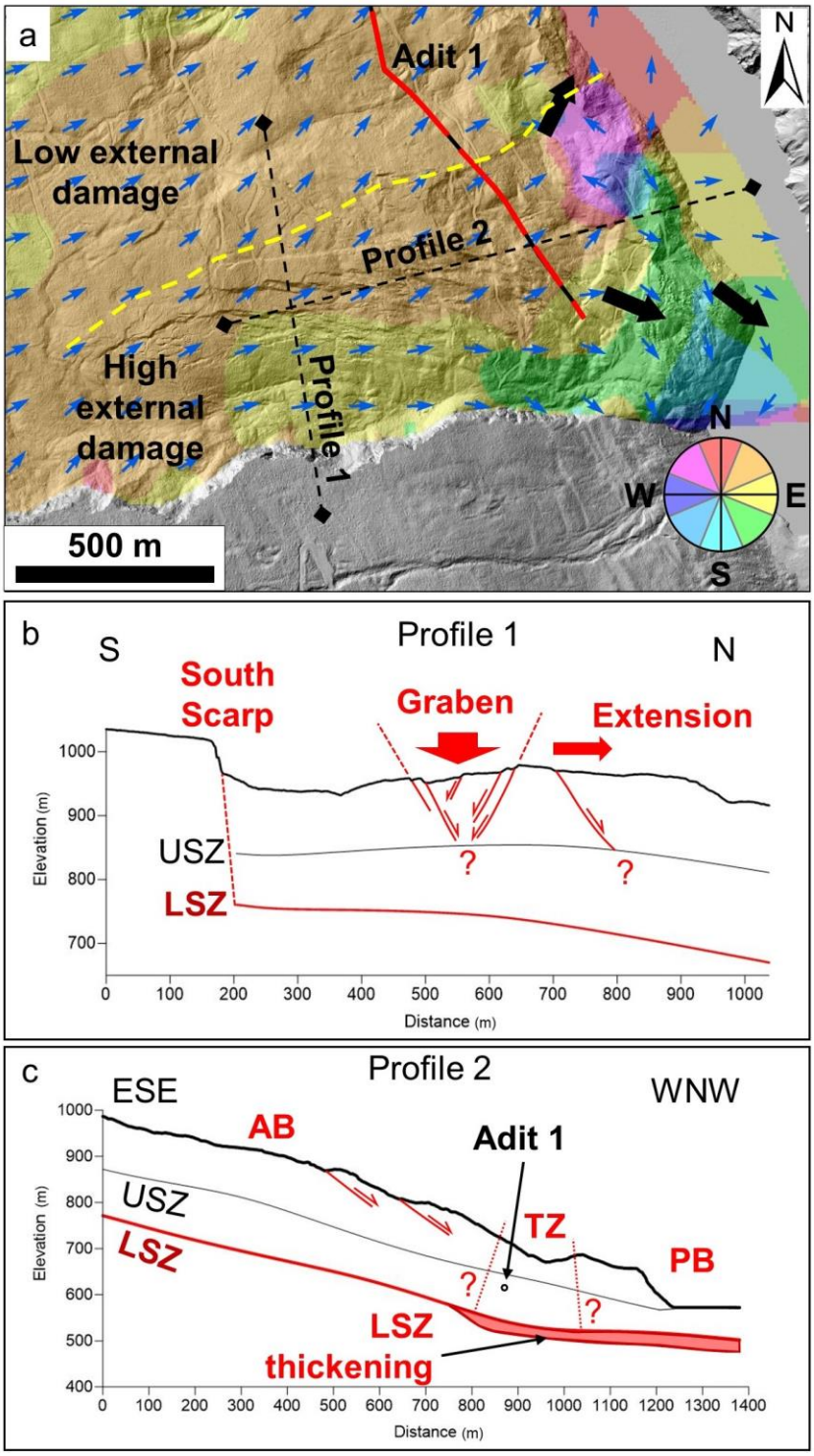

Fig. 18 **Interpretation of slope damage within the southern slope damage domain. a: GIS aspect map overlain on the hillshade map. Blue arrows show the dip direction of the LSZ, and black arrows show the displacement direction in the inclinometers at the LSZ. The solid red/black line is the trace of Adit 1; the red portions are sections where cracking of the shotcrete was observed. b,c: Conceptual sections drawn through the domain. LSZ: lower shear zone; USZ: upper shear zone; AB: active block; PB: passive block; TZ: transition zone (bounded by dotted red lines). [1.5 or 2 column figure]**

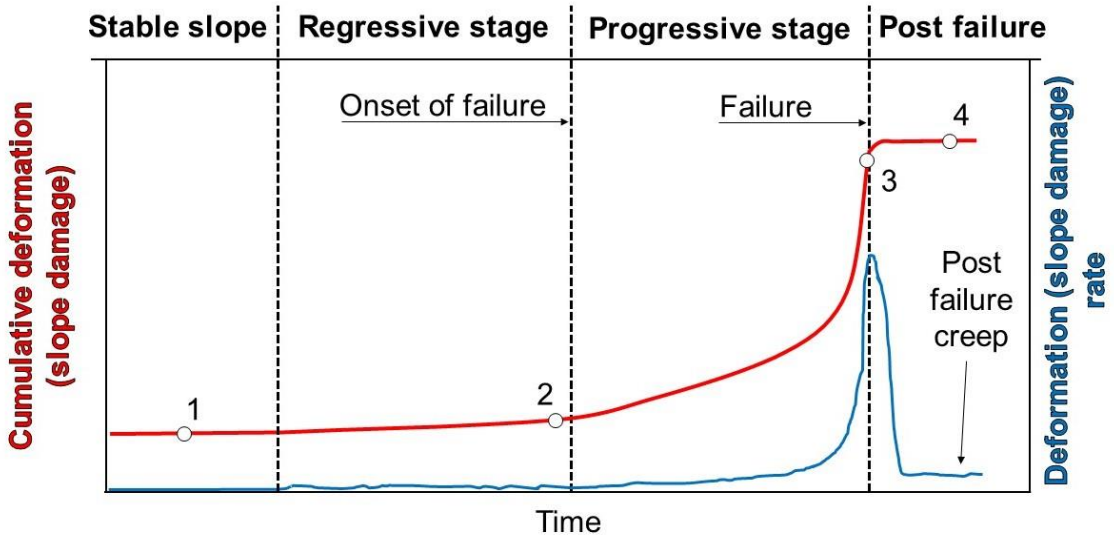

Fig. 19 **Conceptual time-dependent deformation of rock slopes. Note the sharp increase in the rate of deformation and slope damage during the progressive stage, followed by failure. Rock mass creep characterizes the present-day, post-failure state of the Downie Slide. Points 1-4 identify the slope conditions examined in Table 4 (modified from Stead and Eberhardt 2013). [1 column figure]**

Tables

Table 1 **Summary of elevations of the USZ and LSZ in boreholes (see Fig. 4 for location).**

		USZ			LSZ		
ID	Instrument type	Min elevation (m)	Max elevation (m)	Thickness (m)	Min elevation (m)	Max elevation (m)	Thickness (m)
xS-1	-		not identified		451.1	471.8	20.7
S-2	I	606.9	607.5	0.6	492.9	494.7	1.8
S-3	I	903.3	904.7	1.2		not identified	
xS-6	-		not identified		500.2	512.7	12.5
S-7A	I	755.0	763.2	8.2	608.1	627.6	19.5
S-9	I	772.4	775.1	2.7	604.4	619.4	14.9
S-12	I	826.9	830.9	4.0	681.8	689.8	7.9
S-13	P	873.3	875.7	2.4	733.3	751.0	17.7
S-14	I	632.8	636.4	3.7	507.8	545.6	37.8
S-17A	P	501.4	506.0	4.6	463.9	471.2	7.3
xS-18	P		not identified		528.8	534.9	6.1
xS-20	P		not identified		499.6	545.0	45.4
S-21	P		not identified		695.9	706.5	10.7
S-22	P		not identified		597.1	603.2	6.1
S-23A	I	1023.8	1031.1	7.3	913.2	924.5	11.3
S-24	P		not identified		497.7	560.2	62.5
S-26	P		not identified		502.6	522.1	19.5
xS-27	P		not identified		797.7	805.6	7.9
xS-28	P		not identified		645.3	660.5	15.2
S-30A	I		not identified		524.9	554.1	29.3
S-31	P		not identified		889.1	902.5	13.4
xS-32	I		not identified		493.8	509.6	15.8
S-33	P	1287.2	1303.0	15.8	1287.2	1303.0	15.8
S-34	P	1059.8	1067.4	7.6	961.0	975.4	14.3
S-36	P	862.0	867.5	5.5	759.0	761.1	2.1
S-38	P		not identified		569.4	595.3	25.9
S-37	P		not identified		478.8	509.6	30.8
xS-39	P		not identified		504.1	539.5	35.4
xS-40	P		not identified		646.8	656.2	9.4
S-41	P		not identified		570.6	595.0	24.4
S-42	-		not identified		598.0	630.0	32.0
S-43	I	628.8	633.7	4.9	540.4	558.7	18.3
S-44	I	550.5	551.1	0.6	474.9	476.1	1.2
S-45	P	814.4	836.1	21.6	629.4	646.5	17.1
S-49	P	751.6	757.1	5.5	588.9	600.8	11.9
S-51	I	1110.7	1124.4	13.7	994.6	1017.4	22.9

S-52	P	755.3	763.5	8.2	611.4	633.1	21.6
S-54	P	672.1	684.3	12.2	606.9	608.1	1.2

*Instrument types: P: piezometer; I: inclinometer.

Table 2 Summary of displacement rates and direction at depth as recorded by borehole inclinometers.

	USZ		LSZ	
ID	Displacement rate (mm/y)	Displacement azimuth (°)	Displacement rate (mm/y)	Displacement azimuth (°)
S-2	0.50	069	0.45	031
S-12	not detected		0.20	160
S-14	1.00	095	0.79	116
S-23A	not detected		0.15	090
S-30A	not detected		3.18	121
S-32	not detected		0.30	124
S-43	2.00	060	1.10	206
S-44	0.50	074	2.00	077
S-51	not detected		0.70	064

Table 3 Slope damage density (SD_{20}) and intensity (SD_{21}) computed for each of the slope damage domains at the Downie Slide

Slope damage domain	Area (m^2)	Number of features	Cumulative length of features (m)	SD_{20} ($1/m^2$)	SD_{21} (1/m)
Upper distributed damage domain	1,790,300	313	14,800	0.00018	0.0083
Central undamaged domain	895,800	78	4,900	0.00005	0.0054
Northern slope damage domain	1,611,600	491	21,200	0.00030	0.0132
Southern slope damage domain	1,282,700	198	11,700	0.00015	0.0090

Table 4 Proposed model for the evolution of slope damage at the Downie Slide.

	1 – Stable Slope	2 – Regressive stage	3 – Progressive stage	4 – Post-failure stage
Conceptual sketch and section	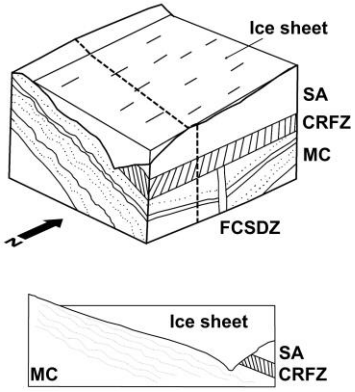	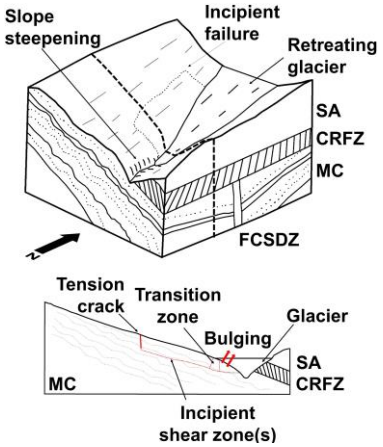	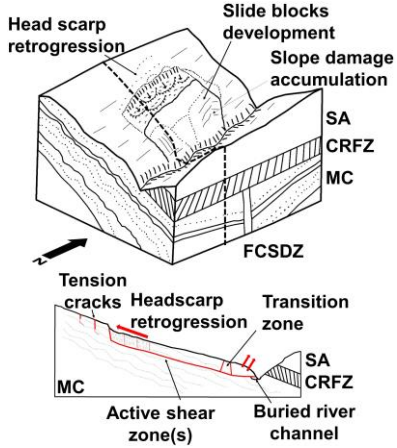	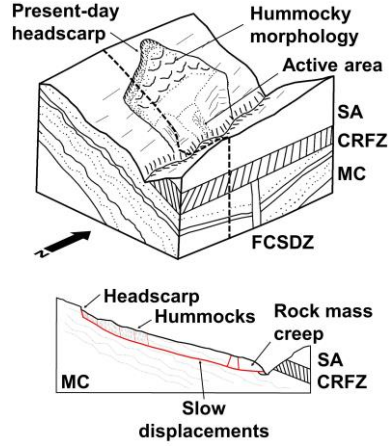
Geomorphic condition	• Ice-covered valley • Buttressed slope	• Deglaciation • Toe of glacially over-steepened slope begins to fail • Slope deformation is favored by high pore water pressures and kinematic release	• Valley is ice-free • Maximum displacement rates • Columbia River shifts, old channel partially buried • Slide expands upslope and laterally • Hummocks form and headscarp gradually retrogresses	• Displacement rates decrease • Surface movements peak at the slope toe • Slow displacements along shear zones; maximum displacements in “active area”
Slope damage evolution	<u>Surficial damage</u> • Insignificant? <u>Internal damage</u> • Insignificant?	<u>Surficial damage</u> • Tension cracks form at the boundary of the unstable area • Bulging at the toe causes cracking and rock mass dilation <u>Internal damage</u> • Incipient shear zone(s) form at the base of the slide • Focused damage accumulates in the Prandtl prism transition zone between passive and active blocks	<u>Surficial damage</u> • Slide body divides into blocks that deform and move semi-independently • Tension cracks form before headscarp retrogresses • Instability propagates to the “lobe” • Surface cracking and dilation occur in northern and southern domains <u>Internal damage</u> • Shear zone(s) thicken due to large displacements • Rock mass dilation and shearing occur in bulging toe and transition zone	<u>Surficial damage</u> • Slumping at the slide toe • Slow deformation induces extension of existing cracks <u>Internal damage</u> • Rock mass deforms slowly (creep) throughout the slide mass and along shear zones

Notes: Dashed lines mark the section traces. SA: Selkirk allocthon. CRFZ: Columbia River Fault Zone. MC: Monashee Complex. FCSDZ: Fissure Creek structural damage zone.